INVESTIGATION INTO HARDNESS CHANGES OF Pd 11.1 AT.% Cu AND Pd 11.1 AT.% Nb AFTER HEAT TREATMENTS

by

Luke Marcus Finkelstein

A dissertation submitted to the faculty of Engineering and the Built Environment, University of Cape Town, in fulfilment of the degree of Master of Materials Engineering

Centre for Materials Engineering
Department of Mechanical Engineering
University of Cape Town
November 2013

Abstract

Two alloys, Pd 11.1 at.% Cu and Pd 11.1 at.% Nb, predicted to form the A_8B ordered structure, were investigated. Prior deformation with systematic heat treatments was used to promote ordering, hardness tests were used to detect changes in the microstructure, which might result from ordering. The Pd-Cu alloy and Pd-Nb alloy did not exhibit any significant hardness changes when heat treated. Transmission Electron Microscopy (TEM) was used to aid detection of any A_8B ordered phase in the Pd-Cu alloy. It was concluded that no ordering had occurred and any initial hardness variation was anomalous. The Pd-Nb alloy was further characterised using Differential Scanning Calorimetry, but no transformation was observed.

The Pd-Cu alloy was predicted by other workers (after commencement of this project) to have a very low ordering temperature, which probably accounts for the lack of ordering at the temperatures reported here. The Pd-Nb alloy is concluded to be extremely slow in atomic rearrangement, so that unfavourable thermodynamics prevented ordering of the alloy during this project.

Acknowledgements

I would like to express my sincere thanks to the following people:

Professor Candy Lang, my supervisor, for making this dissertation a reality with her unparalleled knowledge and guidance.

Penny Park-Ross, for her support in the labs and making sure everything went smoothly.

Miranda Waldron, for her excellent help and guidance with SEM.

Franscious Cummings, for lending me his expertise with TEM.

Chumani Mshumi, for her help with TEM sample preparation and putting up with my numerous questions.

Beverly Glass, for her wonderful administrative support.

To the rest of the staff and students of the Centre for Materials Engineering for all their support and encouragement.

The financial support of the NRF (National Research Foundation) is gratefully acknowledged.

Contents

List of Tables

List of Figures

1. Introduction

In the pursuit of new materials being able to predict whether two elements A and B will form disordered or ordered structures, without having to run numerous experiments, is the key goal of structure prediction[1]. Recently a novel approach has been developed that suggests new structures using geometric simplicity[1], but these theoretical results have not yet been experimentally evaluated. The main objective of the present research is to investigate experimentally two superlattice structures which have been predicted computationally, namely Pd_7Cu and Pd_8Nb superlattices[1-3].

When an alloy of atoms A and B is mixed near stoichiometric compositions (AB, A_3B, A_2B_5, etc.) and heat treated below a certain critical temperature (T_c), it generally forms an ordered structure or superlattice[4,5]. These superlattice formations can change the microstructure of the alloy and these changes can in turn affect the properties of the alloy. Notably one of the changes that is frequently associated with ordering transformations is a change in hardness, brought on by the mechanism of order hardening or by the mixture of the disordered and ordered states[5-7]. By heat treating below T_c, measuring the (micro) hardness of the heat treated samples and monitoring any hardness increase, a first indication of possible ordering can be obtained. The heat treatment conditions which result in the most significant increase in hardness can be enhanced via increased heat treatment time. Samples which have been heat treated in this way can be characterised using Transmission Electron Microscopy (TEM) to determine whether ordering has, in fact, occurred.

Two systems were chosen for the present investigation. Initially the Pd 11.1 at.% Cu alloy was chosen, as there was controversy over whether an A_7B or A_8B structure would be more stable. Recent computational work[2] now shows that the A_7B is more likely; moreover the critical temperature (T_c) for Pd_7Cu is predicted to be -150 °C which presents experimental difficulties in producing an ordered structure. For a second alloy, Pd 11.1 at.% Nb, an A_8B superlattice has been predicted with a T_c of 725 °C[2]. Pd_8Nb has also been predicted by other theoretical methods[3,8]. Neither Pd_7Cu nor Pd_8Nb have been experimentally identified and thus do not feature on their respective equilibrium phase diagrams (as presented in Figure 2.9 and Figure 2.10)[9].

The dissertation is divided into five sections: the literature review which covers previous work conducted, in the context of the work in this dissertation; the experimental methods used, highlighting all steps in the attempted fabrication of the predicted ordered structures; the results gathered through the experimentation, and the discussion and conclusion.

2. Literature Review

This section features a literature review beginning with a short account of structure prediction. It will be followed by sections on superlattices, including their formation mechanisms and kinetics. The next sections focus on the alloying elements used in the present work, with their respective phase diagrams. The final section covers the effects of order hardening.

2.1. Structure Prediction

There are several approaches to predicting alloy structures, from empirical approaches such as Pettifor maps[10], data mining[11] and information theoretic[12,13] methods; to using methods based directly or indirectly on quantum mechanics such as cluster-expansion methods, the coherent approximation methods, bond order potentials and the embedded-atom method[1]. A novel approach that has been designed by Hart[1] predicts binary alloy structures on the basis of geometric simplicity, with the predicted structures having few atoms in the unit cell and those atoms having simple atom-atom interactions[1]. By enumerating the possible structures where the nearest neighbouring atom is unlike (i.e. A-B or B-A) for the first atomic shell and the next-nearest neighbouring atom is like (i.e. A-A or B-B) for the second atomic shell, and taking into account that for face centred cubic structures, the maximum amount of nearest neighbouring unlike atom interactions is 8 out of 12 possible interactions, and the maximum amount of next-nearest neighbouring like atom interactions is 6 out of 6 possible interactions, an algorithm is set up to assign values to the average interactions. These are then summed over the total number of interactions to give the total bond average which measures each structure's relative likelihood of being stable[1,14].

The structures generated by Hart's method include many structures that have already been seen experimentally, such as the common $L1_0$ structure; but a few possible structures that have yet to be experimentally determined have also been predicted, such as Pd_7Mg, Pt_8Mo and Pd_8V[2].

2.2. Ordered Alloys

All alloys can either be ordered or disordered. A disordered alloy is one in which the compositional elements or atoms are randomly positioned on lattice sites in the material, while an ordered alloy has the atom types positioned at specific lattice sites[4]. The process of ordering involves a change from statistically nearly random distributions of atoms among the atom sites into a more regular arrangement, whereby certain sites are occupied predominately by one kind of atom[4]. In a disordered alloy of composition AB, the atoms of A and B have a random chance of occupying a given atom site and it does not matter which one does occupy that atom site, but upon ordering the A and B atoms can segregate more or less completely to specific atomic sites in an arrangement that can be described as a lattice of A atoms interpenetrating a lattice of B atoms. This may take place with little or no distortion of the lattice, creating an ordered solid solution which is also known as a superlattice or superstructure[4,5,15,16]. Ordered alloys form below a critical ordering temperature (T_c) which differs from the alloys melting temperature[4].

2.2.1. Long Range Order

The formation of superlattices is frequently described as long range order and follows the configurational trend of superlattices put forward in section 2.2 above[4,5]. There are two types of LRO: permanently ordered alloys, which have a T_c greater than or equal to the melting temperature of the alloy, and reversibly ordered alloys, which have a T_c less than the melting temperature of the alloy[17,18]. The degree of long range ordering (S) depends on the amount of undercooling from T_c where a higher amount of undercooling leads to a higher amount of ordered phase and can be represented with the following equation where p increases as undercooling increases[4]:

$$\mathbf{S = (p – r) / (1 – r)} \qquad \text{(Eq. 1)}^{4}$$

Where:

S = degree of long range order (Bragg-Williams parameter)

p = probability of an A atom occupying an A atomic site

r = fraction of ‘n’ total sites occupied by A atoms for complete order

In ordered structures, where S is a value between 0 and 1, different atomic configurations are possible. One possibility is a single long range scheme that has occasional atoms out of place on the atom sites of the crystal[4]. Another possibility is that of many domains where each has their own long range scheme of perfect or partial order, but each domain has an arrangement of atoms out of step with the arrangement in each adjacent domain[4]. Also, there may or may not be a two-phase arrangement, in which a partially ordered phase coexists with a disordered phase (or with a partially ordered phase of a different superlattice structure)[4]. This can lead to the formation of antiphase domain boundaries by the growing together of different nuclei of order[4]. Antiphase domain boundaries can also be generated by the passage of a dislocation through an ordered crystal[4]. These antiphase boundaries have an effect on hardness and are discussed in section 2.11.1.

2.2.2. Short Range Order

While S describes the long range order in crystals with the A and B atoms ordering into a superlattice, there can also be the case where the AB atom relationship can occur in a nearest neighbour type of interactions. This kind of ordering is known as short range order (SRO)[4,19]. SRO can occur above and below the T_c temperature, and can be thought of as an unexpected increase in ordering (more AB bonds than AA or BB) in a disordered matrix[15,16,19,20]. Four models have been proposed which all differ in homogeneity, heterogeneity and stability[19]. They are the statistical short range order model, the disperse short range order model, the microdomain short range order model and the lattice defect order model[19,21].

2.3. Superlattice Formation

There are many different ways in which two elements in a binary solution can be arranged[5]. These include the most common which is the almost random distribution, where statistical preferences for like or unlike neighbours are certain to be present[5]. Also included is the intermetallic compound, where the different atoms are located on distinct lattice sites; this type of structure retains its ordered configuration to the melting point of the alloy, and occurs at or near the stoichiometric compositions[5]. The next set of alloys falls between the previously mentioned groups of alloys, and has a sharply defined critical temperature, known as the critical ordering temperature (T_c)[5]. Below T_c the atoms have a strong preference for specific lattice sites (typically called long range order), while above T_c a random solid solution is present although small domains of unlike nearest neighbours (typically called short range order) are found to exist[5]. This set of alloys is known as ordered alloys, with the ordered structure forming below T_c commonly known as a superlattice or superstructure[5]. Superlattices form at relatively low temperatures when compared with their melting points and, like intermetallic compounds, form at or near simple stoichiometric compositions such as AB, A_3B, AB_4, etc. but can have a wide (compositional) range of stability which is not typical of intermetallics[5]. Superlattices were theorised by Koehler[22] who predicted they would have increased mechanical resistance, which has been proven[15,23,24].

2.4. Mechanisms of Superlattice Formation

The transient characteristics of an ordered alloy, after being undercooled below the critical ordering temperature, depend on the ordering mechanisms which are operative as equilibrium is approached[5]. An ordering mechanism cannot be deduced from the equilibrium state therefore the mechanism is selected from a number of possible ordering mechanisms[5]. Even though an ordering transformation is thermodynamically possible, the ordering mechanism that will operate is the one that is kinetically most favoured in overcoming the activation energy barrier[5].

There are two main types of ordering mechanisms: drastic atomic rearrangements within very small localised volumes (Type I transformations), and very small atomic rearrangements which are spread over large volumes (Type II transformations)[5]. Therefore a heterogeneous reaction (nucleation and growth) will be classified as a Type I change, while homogeneous reactions are classified as Type II[5]. This distinction is very useful in the case of a system where nucleation and growth is on a very fine scale; then though it is inherently a Type I reaction, it would be experimentally indistinguishable from a homogeneous, i.e. Type II reaction[5].

2.4.1. Type I Transformations

For this type of transformation, small ordered regions are nucleated at random points within the sample and these centres then grow at the expense of the disordered phase by the independent transference of atoms at the boundary, the rate being temperature dependent[5]. A sharp interface separates the transformed phase from the original phase; such a reaction is diffusion-controlled and the curves characterising TTT (time-temperature-transformation) behaviour are C-shaped[5]. At times, the new phase grows at sites where preferential nucleation (of the previous phase) had previously taken place[5]. By convention, growths starting at specific sites such as grain-boundaries, dislocations, etc., are characterised as heterogeneous nucleation events but in the realm of ordering transitions, a heterogeneous reaction refers to transformation in discrete localised regions, not necessarily at sites of crystal imperfections[5].

2.4.2. Type II Transformations

For this type of transformation, heating below the critical ordering temperature causes the superlattice to simultaneously form at all points within the sample[5]. The only change with increased annealing time (isothermal) is that the degree of order increases uniformly. At no stage of the cycle do ordered and disordered materials exist side by side. Under equilibrium conditions, the final lattice would be indistinguishable from Type I transformations, but the temporary structures are completely different[5].

In some alloys the ordering reaction cannot be readily categorised as either Type I or Type II. Cu_3Au is an example of a Type I reaction but ordering can also occur homogeneously (Type II) in this alloy when the annealing temperature is lowered[7]. In another example, Fe_3Al orders homogeneously on continued cooling (Type II), and orders isothermally by nucleation and growth (Type I)[7]. From the results of measured quantities, in almost every ordering system, little doubt remains that the processes involved, regardless of the mechanisms which are operative, are diffusion-controlled[5].

2.5. Kinetics of Superlattice Formation

The rate at which a superlattice will form depends on atomic diffusion. Several factors influence atomic diffusion, including temperature, vacancy concentration (via defects) and composition.

The Arrhenius equation is well known for describing all thermally-activated processes, including diffusion. The energy barrier for atomic diffusion is the energy barrier for atomic movement, which requires a sufficient temperature to overcome. There are two mechanisms for atomic movement in crystal lattices: vacancy and interstitial diffusion. For vacancy diffusion, vacancies are needed to allow atomic movement by substitutional diffusion. Additional vacancies may be introduced via defects, which can be created from irradiation, quenching from high temperatures or plastic deformation. Plastic deformation also provides a variety of other defects such as dislocations, jogs and stacking-faults. Dislocations have been found to be favourable nucleation sites for ordered domains, which results in faster and coarser precipitation of new ordered phases[25,26]. It is useful to note that the high internal stresses produced by deformation also induce preferential domain alignment which can result in a higher degree of order[25,26]. It should also be noted that while vacancies produced by deformation can have a positive effect on ordering kinetics and the degree of order, there is also a negative effect of vacancy sinks such as dislocations[27,28]. The interaction of dislocations and solute atoms may also produce a solute flux to dislocations which lowers the solute fraction necessary for precipitation of a new phase[29].

2.6. Superlattice Structures

The bulk of superlattice structures are related to three principal metallic structures, the face centred cubic (A1 or FCC), the body centred cubic (A2 or BCC) and the hexagonal close packed (A3 or HCP)[4]. To refer to specific superlattice types it is common to use their *Strukturbericht* designations, for example the $L1_0$, the $L1_1$ and $L1_2$. Some examples are shown in Figure 2.1.

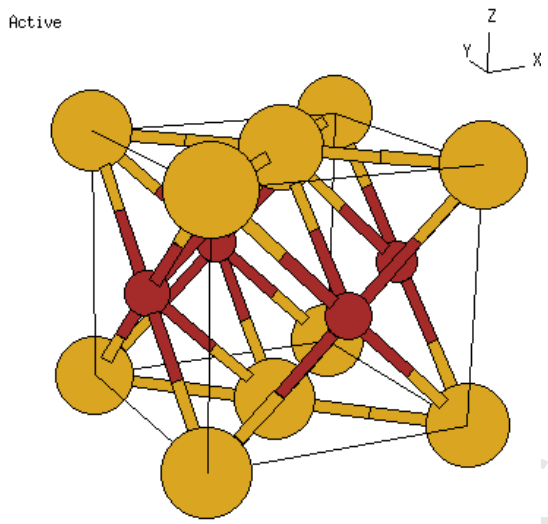

a) $L1_0$ e.g. AuCu

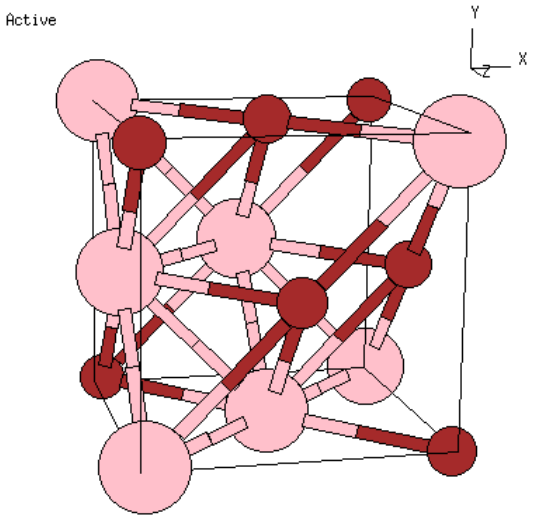

b) $L1_1$ e.g. CuPt

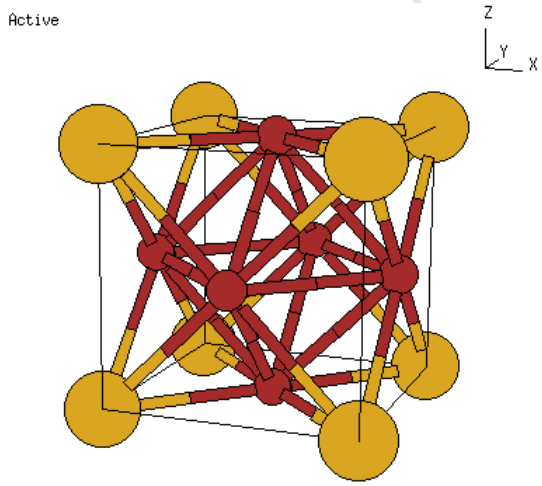

c) $L1_2$ e.g. Cu_3Au

Figure 2.1: Examples of typical *Strukturbericht* designations (after NRL crystal structures website[30])

2.6.1. The A_7B Superlattice

Figure 2.2 shows a typical A_7B type superlattice, the Ca_7Ge structure[30]. The lattice is in the space group Fm-3m with the space group number 225, and has a Pearson symbol of cF32. Other compounds with this structure are Pt_7Li, Zn_7Mo and Pt_7Cu[23,30]. It is reported that the A_7B structure is not easily distinguishable from the structure ABC_6 predicted by Tang[31] on the basis of using X-Ray Diffraction (XRD) for the case of the Pt-Cu alloy[23]. Work by Carelse and Lang[23] on the Pt 14 at.% Cu alloy show TEM diffraction patterns at different stages of ordering the Pt_7Cu structure, which are shown in Figure 2.3.

.

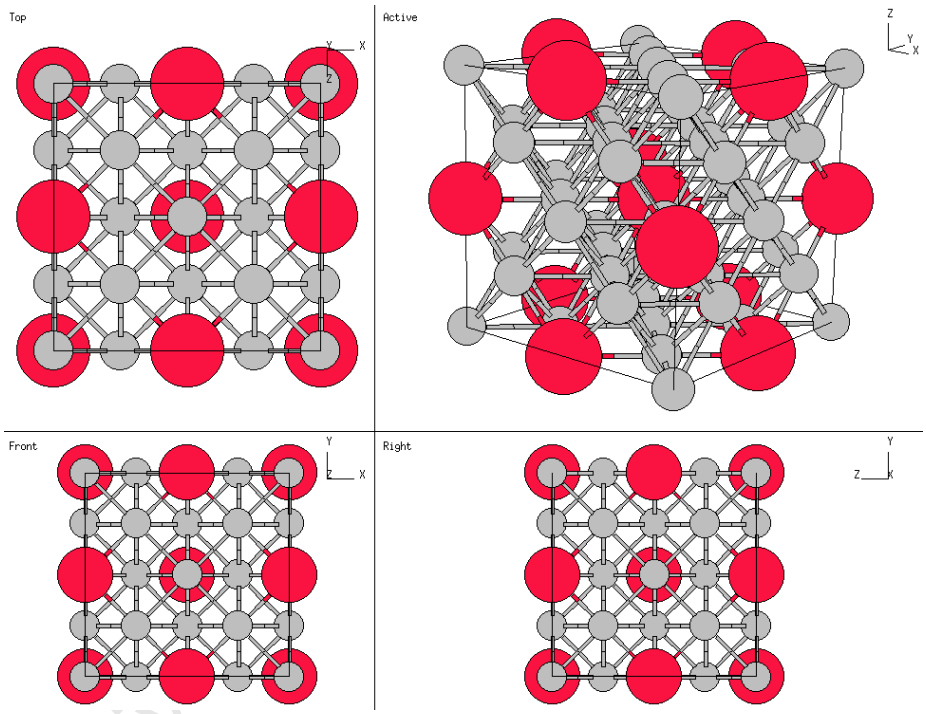

Figure 2.2: A_7B type superlattice represented by Ca_7Ge (after NRL crystal structures website[30])

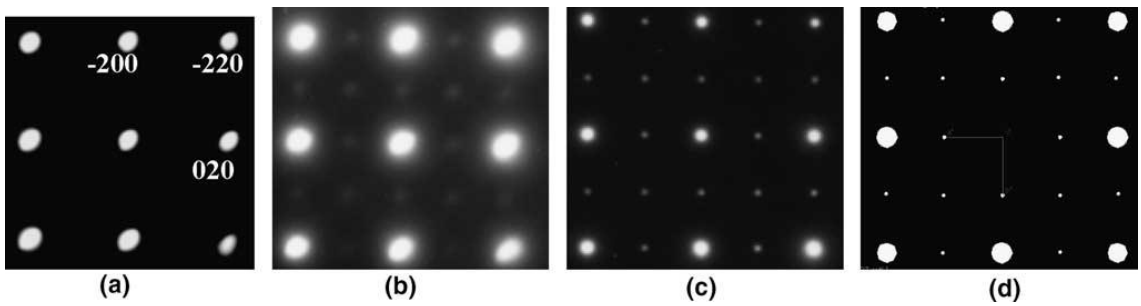

Figure 2.3: Electron diffraction patterns of Pt 14 at.% Cu viewed along the [001] zone axis: (a) disordered sample, (b) initially cold worked sample after heat treatment at 200 °C, (c) initially quenched sample after heat treatment at 200 °C and (d) simulated electron diffraction pattern for $CuPt_7$ (After Carelse and Lang[23]).

2.6.2. The A_8B Superlattice

Figure 2.4 shows a typical A_8B type lattice, the Ni_8Nb structure[30]. The Bravais lattice for the structure is body centred tetragonal (bct) and has the prototype Pt_8Ti[15,32]. The A_8B structure can occur when A is an element from groups 4 to 6 (Ti, Zr, Hf, V, Nb, Ta, Cr, Mo or W) and B is an element from Group 10 (Pt, Pd or Ni)[3,15]. The lattice is generally described as face centred tetragonal (fct) for ease of comparison with the parent platinum based solid solution which is face centred cubic (fcc)[15,32-34]. The lattice is in the space group I4/mmm with the space group number 139, and has a Pearson symbol of tI18[30]. Work by Nxumalo and Lang[35] on the Pt 11 at.% V alloy show ordering of Pt_8V in TEM diffraction patterns on zone axes [100] and [110], which is shown in Figure 2.5.

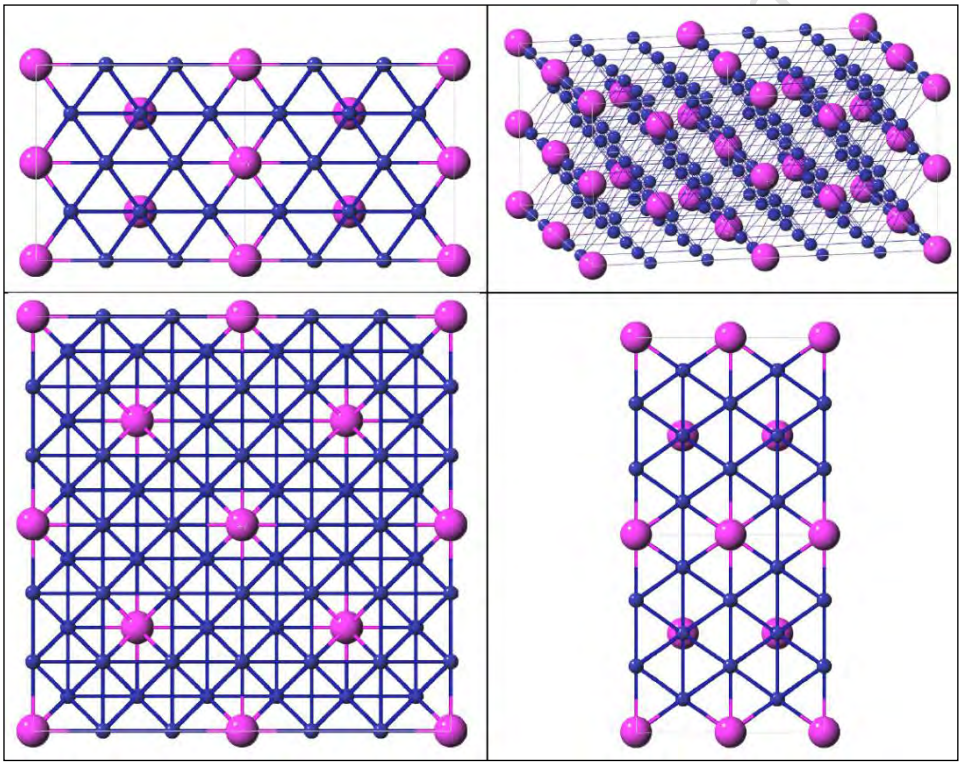

Figure 2.4: A_8B type superlattice represented by Ni_8Nb (after NRL crystal structures website[30])

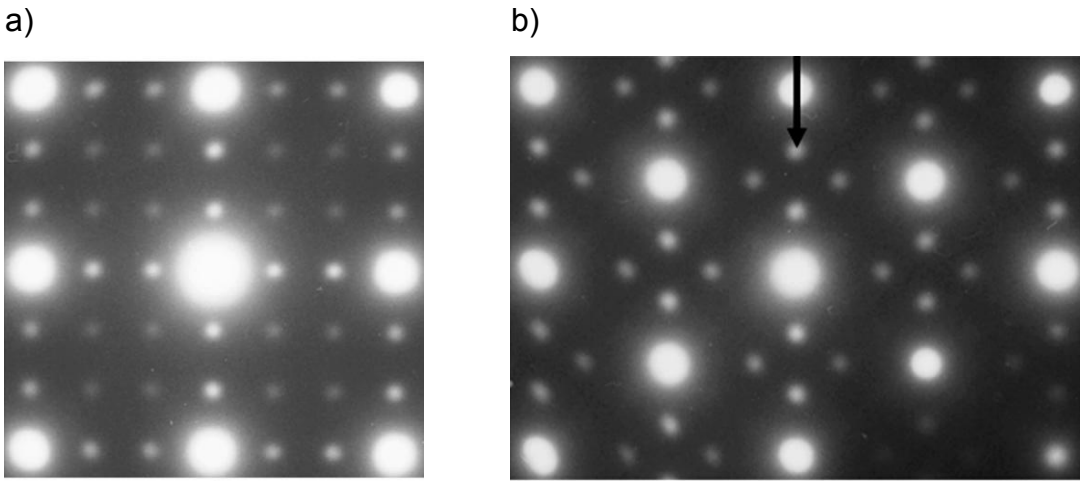

Figure 2.5: TEM diffraction patterns of initially quenched Pt 11 at.% V after heat treatment for 3 hours at 600 °C, (a) [100] and (b) [110] zone axes (after Nxumalo and Lang[35])

2.7. Elements Pt, Pd, Cu and Nb

2.7.1. Platinum (Pt)

Platinum (Pt) is a transition metal, and belongs to the group of elements called platinum group metals (PGMs), which includes rhodium, iridium, palladium, osmium and ruthenium[36]. Table 2.1 summarises the physical and crystalline properties of platinum. Platinum does not oxidise at any temperature below T_m but is corroded by halogens, cyanides, sulphur, and caustic alkalis. It is insoluble in hydrochloric and nitric acid, but dissolves in aqua regia to form chloroplatinic acid, H_2PtCl_6. Platinum forms many stable alloys with other metals, including most of the other platinum group metals[37]. Some of the applications of platinum are its use in industry as a catalyst to produce nitric acid and chlorine; it is also used as a hetero- and homogenous catalyst in organo-metallic chemistry which finds uses in the petroleum industry[38,39]. Platinum is also used as a catalyst in car exhausts to reduce CO_2 emissions and more recently platinum has been applied as a catalyst to fuel cells in efforts to find viable alternative fuel sources[38,39]. Platinum is also used in jewellery due to its attractive physical properties[39].

Table 2.1: Physical and Crystalline Properties of Platinum, Palladium, Copper and Niobium[36,40,41]

Property	Platinum	Palladium	Copper	Niobium
IUPAC symbol	Pt	Pd	Cu	Nb
Atomic number	78	46	29	41
Atomic weight	195.09	106.42	63.546	92.906
Atomic radii (pm)	177	169	145	198
Group number (IUPAC)	10	10	11	5
Period number (IUPAC)	6	5	4	5
Melting point [°C]	1768	1552	1084.62	2477
Boiling point [°C]	4530	3980	2927	4744
Density at 20°C [g/cm^3]	21.45	12.023	8.92	8.57
Thermal conductivity at 0 to 100°C [W/mK]	71.50	71.8	400	54
Electrical resistivity at 20°C [μΩcm]	10.58	10.54	1.72	15.2
Co-efficient of linear thermal expansion at 0 to 100°C [10^{-6}/K]	9.0	11.8	16.5	7.3
Vickers hardness [MPa]	549	461	369	1320
Crystal structure	FCC	FCC	FCC	BCC
***Strukturbericht* designation**	A1	A1	A1	A2
Pearson symbol	cF4	cF4	cF4	cI2
Lattice spacing [Å]	3.916	3.8830	3.6149	3.3004
Space group	Fm-3m	Fm-3m	Fm-3m	Im-3m
Space group number	225	225	225	229

2.7.2. Palladium (Pd)

The physical and crystalline properties of palladium are summarised in Table 2.1. Palladium dissolves slowly in sulphuric, nitric, and hydrochloric acid, and does not react with oxygen at ordinary temperatures. Palladium heated to 800 °C will produce a layer of palladium(II) oxide (PdO). It does however lightly tarnish in a moist atmosphere containing sulphur[37]. Palladium has applications similar to platinum (autocatalyst, industrial and jewelry)[39]. Palladium is also used for hydrogen storage and purification of hydrogen from other gases[42].

2.7.3. Copper (Cu)

The physical and crystalline properties of copper are summarised in Table 2.1. It is an abundant metal and is commonly used for its good electrical and thermal conductivity[37,41]. Copper is widely used as an alloying element, most notably in alloys with zinc (brass), tin (bronze), nickel plus zinc (german silver also known as nickel silver) and silver (sterling silver)[41].

2.7.4. Niobium (Nb)

The physical and crystalline properties of niobium are summarised in Table 2.1. Niobium is also known as columbium, and has a shiny white lustre. It has chemical and physical properties similar to Tantalum (Ta) and the two elements are therefore hard to distinguish[40]. Niobium finds most use in stainless steels as an alloying element, but is also used in the nuclear industry and is found in some magnets and superconducting magnets[40].

2.8. The Platinum-copper System

The platinum-copper phase diagram is shown below in Figure 2.6; which shows the ordered phases Cu_3Pt, one long period superlattice (LPS) and CuPt[9]. The existence of the Pt_3Cu ordered phase has also been established[43]. A model for the A_7B ordered structure formed by Pt 12.5 at% Cu, Pt_7Cu, was first proposed by Schneider and Esch[44], as shown in Figure 2.7(a). Tang[31] proposed a similar model for platinum containing from 12 at% copper to 25% at% copper, as shown in Figure 2.7(b). Tang's Model is better known as the ABC_6 ordered structure, and was initially proposed as the model for the ordered structure around platinum 25 at% copper[23]. The Pt_7Cu ordered structure is of interest as it might be an analogous material to the possible Pd_7Cu ordered structure. Heat treatments conducted by Carelse and Lang[23] on cold worked Pt 14 at.% Cu showed a substantial increase in hardness. The hardness data can be seen in Figure 2.8, with the increased hardness peaking at the 200 °C heat treatment. The ordered Pt_7Cu phase was shown to form below 500 °C, resulting in a heterogeneous structure of ordered domains in a disordered matrix[23]. The higher hardness in the initially cold worked and heat treated samples, with a domain size of 5 to 10 nm[23], is consistent with Stoloff and Davies' observation that a peak in hardening occurs at a domain size of approximately 6 nm[7,23]. It was noted after long heat treatments that the domain size of the initially cold worked samples remained relatively the same size due to the annihilation of vacancies due to vacancy sinks such as dislocations, as the vacancies would migrate to nearby sinks in the early stages of heat treatment[23]. This would lead to a significant reduction in diffusion and hinder further growth of the ordered domains[23].

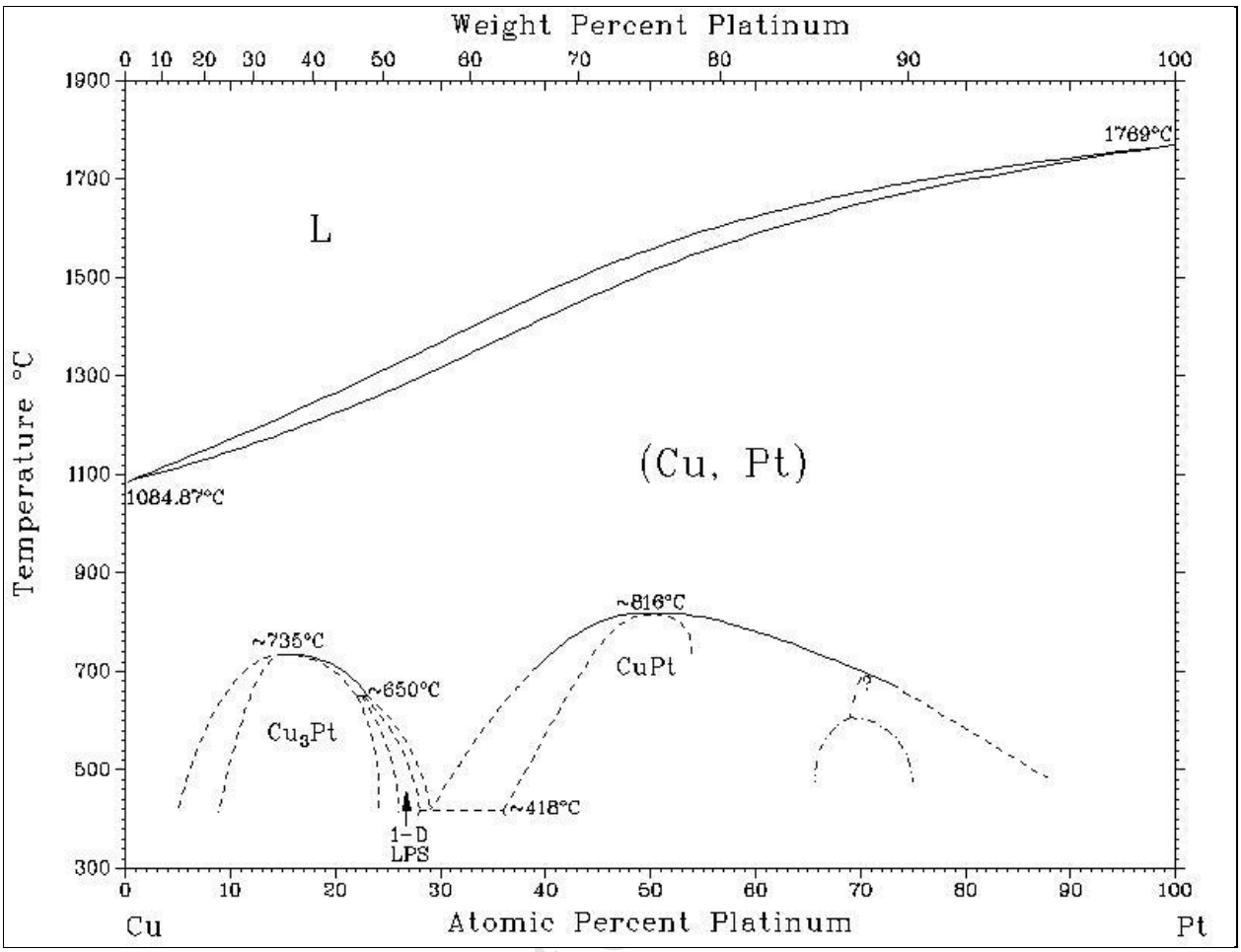

Figure 2.6: Pt-Cu equilibrium phase diagram (after ASM International: Binary Phase Diagrams[9])

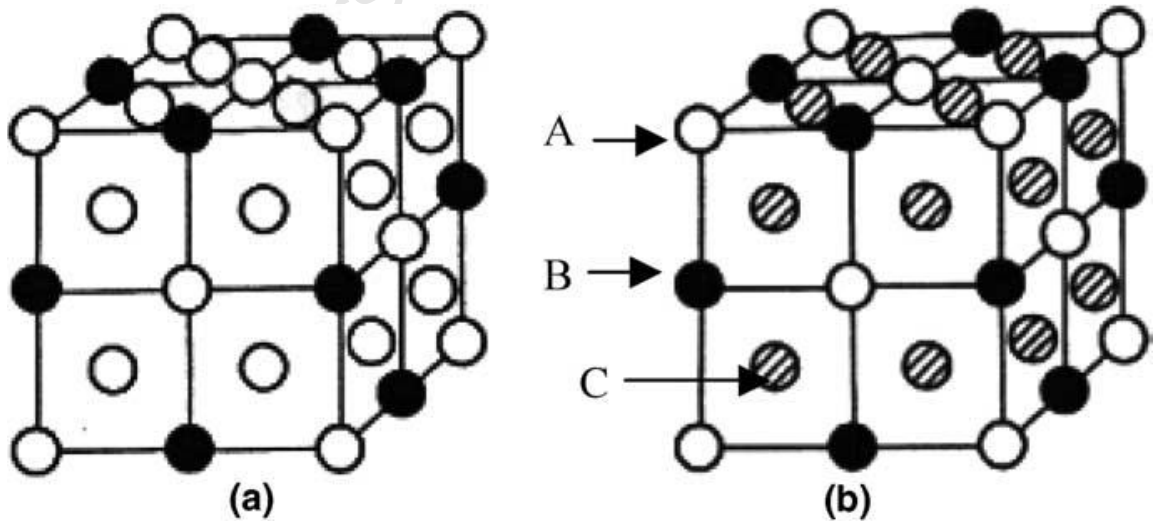

Figure 2.7: (a) Schneider and Esch's model (A_7B structure) and (b) Tang's model (ABC_6 structure) (after Schneider and Esch[44], and Tang[31] respectively)[23]

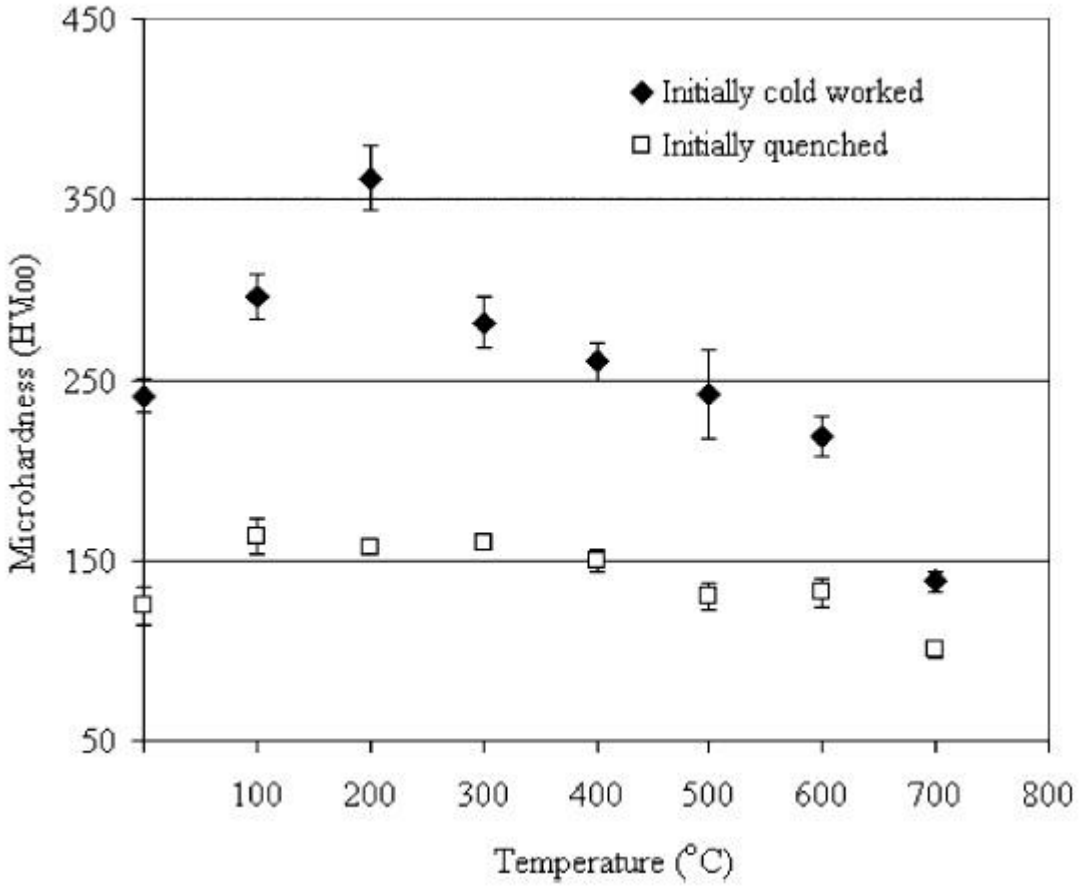

Figure 2.8: Hardness vs. heat treatment temperature for initially cold worked and initially quenched Pt 14 at.% Cu after heat treatment for 3 hours (after Carelse and Lang[23])

2.9. The Palladium-copper System

The phase diagram of the Pd-Cu alloy system is shown in Figure 2.9[9]. The equilibrium phases present in the Pd-Cu system are: the liquid, L; the fcc continuous solid solution, (Cu,Pd); the ordered $L1_2$-type phase Cu_3Pd (α'), the ordered Cu_3Pd (α'') and the ordered phase PdCu, all existing in the solid solution phase field[45,46]. The ordered phase Cu_3Pd (α') occurs over the composition range of 10 to 20 at% Pd, with a maximum transformation temperature of 500 °C at the off-stoichiometric composition of 15 at%, while the alloys that form from 20 to 25 at% Pd have a tetragonal structure[45,46]. The Cu_3Pd (α'') has a one-dimensional antiphase domain (1D APD) structure (or Long-period Superlattice. LPS) in alloys with composition ~17 to ~28 at% Pd and a "complex" APD structure in ~19 to ~31 at% Pd alloys[45-47]. These APD structures have a fundamental unit cell which consists of a face-centred tetragonal (FCT) atomic arrangement of the ordered Cu_3Au-type structure[45,47].

These structures have long been the source of controversy but recent work by Baerthlein *et al* suggests that the 2-D LPS structures are likely kinetically stabilised structures which should decompose into the 1-D LPS ground-state structures at thermodynamic equilibrium, but the decomposition is suppressed by kinetic barriers[48]. Their work is able to describe the complex SRO behaviour of the Pd-Cu system, in agreement with earlier experimental investigations[43,48,49]. The PdCu (β) ordered alloy has the CsCl-type (B2) ordered structure and is observed over the range 36 to 46 at% Pd and occurs up to a maximum temperature of 596 °C at the off stoichiometric composition of 40 at% Pd[45,47]. No ordered structures above 58 at% palladium are shown on the phase diagram. The Pd-Cu system has local clustering at 950 °C, which is different from its analogue alloy, Pt-Cu, which shows short range ordering near that temperature[50].

Recent work by Hart *et al* shows a predicted A_7B ($CuPt_7$-type) superlattice near 87.5 at.% Pd, with a predicted T_c of approximately -150 °C[2].

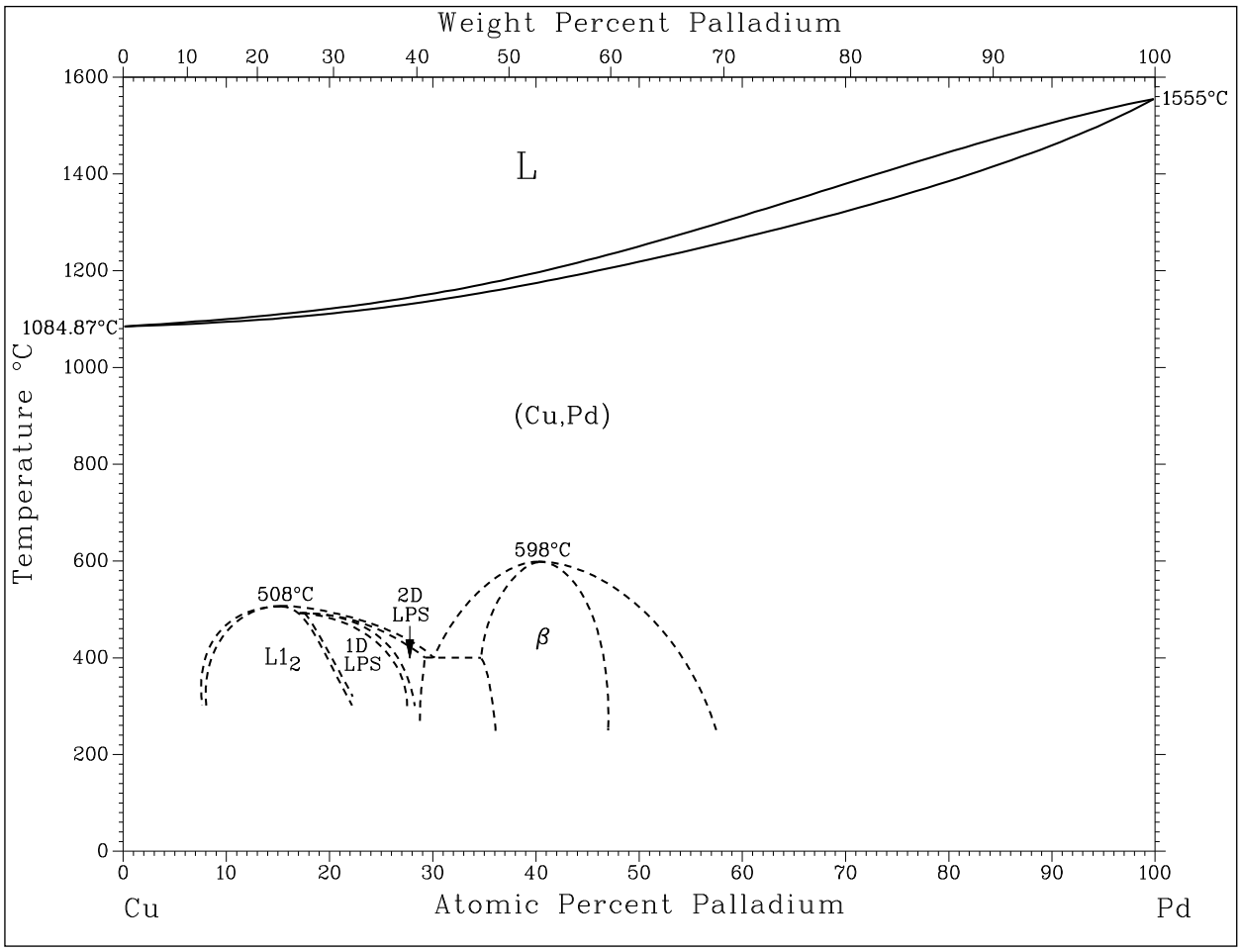

Figure 2.9: Pd-Cu equilibrium phase diagram (after ASM International: Binary Phase Diagrams[9])

2.10. The Palladium-niobium System

Palladium–niobium alloys form ordered structures up to high temperatures, as shown in Figure 2.10. To date NbPd, $NbPd_2$ and $NbPd_3$ ordered structures have been documented[9,51]. The NbPd ordered structure has a high-temperature disordered Cu-type structure and is stable between 1565 and 1255 °C, exhibiting solubility at 49 to 60 at% Pd in the high-temperature end. The $NbPd_2$ ordered structure has an orthorhombic $MoPt_2$-type phase, with a very narrow solubility range between 66 and 67 at% Pd. There are two $NdPd_3$ phases, a low-temperature α-$NbPd_3$ with BCT Al_3Ti-type structure, and an orthorhombic β-$NbPd_3$, formed from Pd through a eutectoid reaction at 1560 °C[9,51]. The two forms are related structurally but the phase transformation between them is not fully established; experimental work on the two $NbPd_3$ phases by Giessen *et al*[51] is shown in Figure 2.11 where data has been collected[9]. Figure 2.11 sheds some light on the $NbPd_3$ phase but is incomplete according to Giessen *et al*[51]. The liquidus boundary, especially on the Nb-rich side of the diagram, has not been accurately determined and therefore is shown by a dashed line[9]. No ordered structures are shown above 82 atomic percent palladium on the phase diagram.

Recent work by Hart *et al*[2] shows a predicted ordered A_8B (Pt_8Ti-Type) superlattice with a predicted T_c of approximately 725 ^oC.

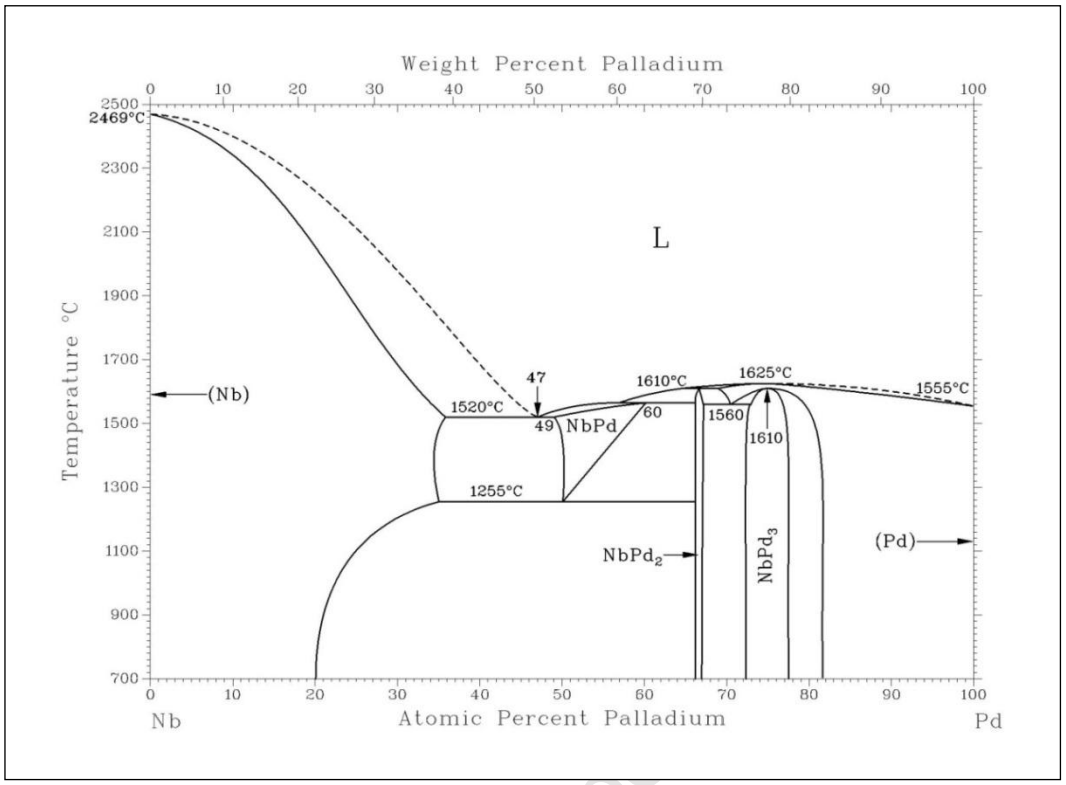

Figure 2.10: Pd-Nb equilibrium phase diagram (after ASM International: Binary Phase Diagrams[9])

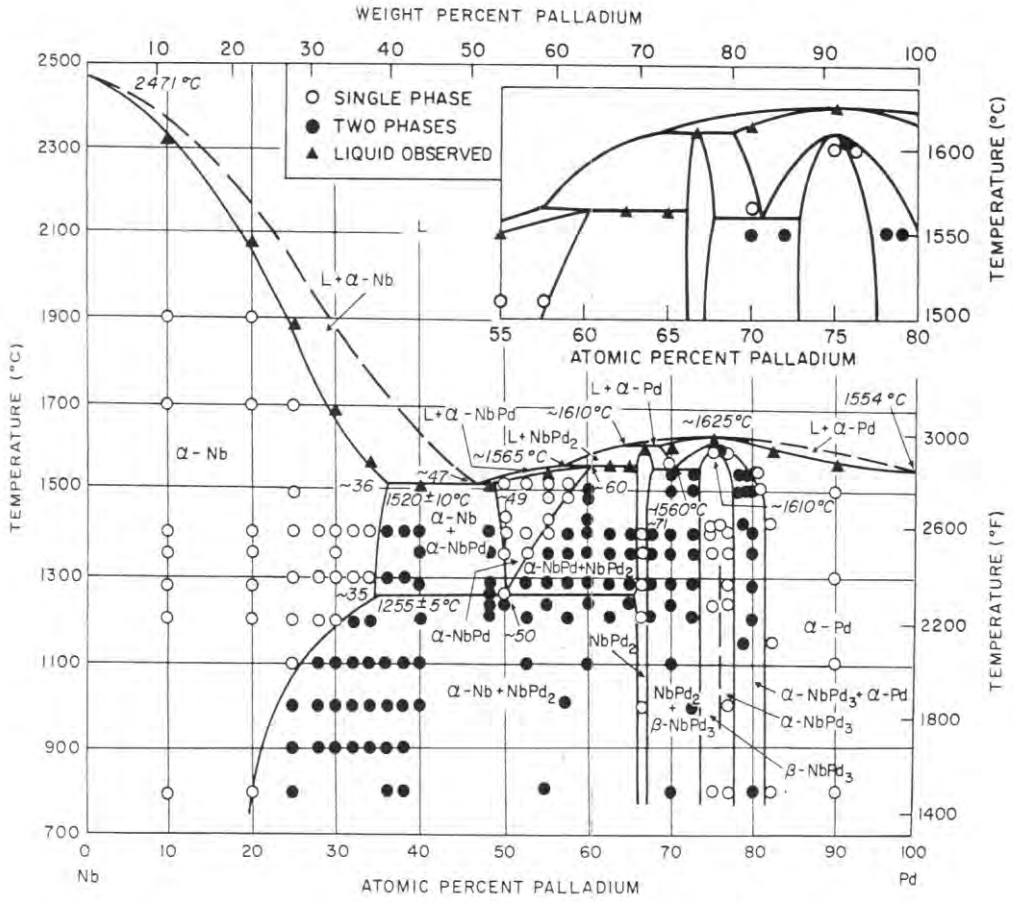

Figure 2.11: Proposed Pd-Nb constitution phase diagram (after Giessen *et al*[51])

2.11. Strengthening Mechanisms

The movement of dislocations in a ductile material will cause plastic deformation, but anything that inhibits their movement increases the stress required for further deformation[52]. There are several mechanisms such as the well-known work hardening or strain hardening mechanism, where deformation is applied to a ductile material so that the dislocation density increases which in turn increases the interactions these dislocations have with each other, and therefore causes an increase in the amount of stress required for further deformation[52]. These dislocations are non-equilibrium defects and will undergo rearrangement and annihilation when sufficient energy for rapid solid state diffusion is available, in order to reduce the free energy of the material[52]. For this research, two mechanisms will be discussed in the following sub-sections, namely order hardening and dispersion hardening.

2.11.1. Order Hardening

It is well known that ordering transformations can lead to hardening and strengthening of alloys and various strengthening models have been proposed[5,7,15]. Ordering processes that have a change of symmetry lead to a significant change in hardness, while structure variables such as incomplete order, antiphase domain boundaries and paired dislocations control the effect of order on hardness[5,7,16]. A change in strength may arise from long range order, involving a complete transformation of the disordered alloy to a superlattice structure; or from a partial transformation to a mixed state containing ordered domains in a disordered or short-range ordered matrix[15]. Another of the proposed mechanisms for long range order hardening is the formation of superdislocations, of which the most common form is the paired dislocation[5,7,15]. The reason for the formation of paired dislocations is that a single dislocation passing through a lattice causes disordering (from ABAB to AABB) and therefore to restore ordering another dislocation is needed to pass through the lattice, which creates an antiphase boundary between the two dislocations (a ribbon of sorts), which in turn increases the hardness of the alloy as both dislocations are now necessary thus increasing the stress required for deformation[5,16]. For A_8B structures another superdislocation type, the triple dislocation, can be seen as in the case of Pt_8V[53].

There can also be a change, with deformation, to a purely statistical preference for unlike nearest neighbours (AB atom pairs) explained by the statistical short range order model[4,19]. The mechanism for short range order hardening most commonly seen in platinum-type metals can be seen as analogous to precipitation hardening where small domains of different hardness inhibit dislocation movement. SRO hardening therefore occurs from the dispersion of ordered domains within a disordered alloy matrix and it is these domains that inhibit dislocation movement which in turn increases the hardness of the alloy[15]. Irani and Cahn[6] suggested that all order strengthening models should contain the central concept of a maximum flow stress at an intermediate degree of order, as this is the most common factor observed experimentally[15]. More recent work on order strengthened alloys has focussed on alloys which are strengthened by the presence of coherent ordered precipitates in a disordered matrix, such as the nickel-based superalloys and aluminium-lithium alloys[15,24].

2.11.2. Dispersion Hardening

Often in materials containing more than one phase, one of these phases may be distributed within the material as fine particles. This dispersion of small particles has the effect of increasing the strength of the material by an amount which depends on the volume fraction and size of the particles[52]. These small particles cause an approaching dislocation to bow between the particles, as the dislocation cannot cut through them, thus requiring more stress for the dislocation to move.

A dispersion of these fine particles may be produced using a number of methods such as internal oxidation or by heating a metastable solid solution so that a second phase precipitates[52,54]. The latter method is known as precipitation hardening and is seen quite readily in certain Al-Cu alloys[52]. Recently the use of nanoscaled oxide ceramic powders in metal micropowders through mechanical alloying has shown increased hardness over their pure metal counterparts, and is useful for situations where dispersion-strengthened metals are required but internal oxidation is not applicable, e.g. magnesium[54].

For precipitation hardened systems the particles may be metastable and form a coherent interface with the matrix[52]. The metastable precipitates may just be small clusters of only 100 solute atoms or may have a developed crystal structure that differs from the matrix[52]. The coherent interface that is formed in the material creates elastic strains within, known as coherency strains, and dislocations interact with the strain field similarly to elastic strains around a solute atom but with a stronger effect[52]. Also dislocations may cut the particles instead of bowing past them, which creates new precipitate-matrix surfaces[52]. These new surfaces are associated with an energy per unit area value and thus require a higher stress to move the dislocations[52]. The combination of these two effects greatly increases the strength of the material.

3. Experimental Method

The Pd 11 at% Cu and the Pd 11 at% Nb alloy buttons were fabricated at Mintek via arc melting. A sample from the Pd 11 at% Cu and the Pt 11 at% Nb alloy buttons was retained and labelled as the 'as cast' condition for hardness comparisons. The remainder of the alloy buttons were cold rolled to promote subsequent homogenisation in a vacuum furnace, with an argon atmosphere to minimise oxidation. Figure 3.1 below outlines the method in flow chart form.

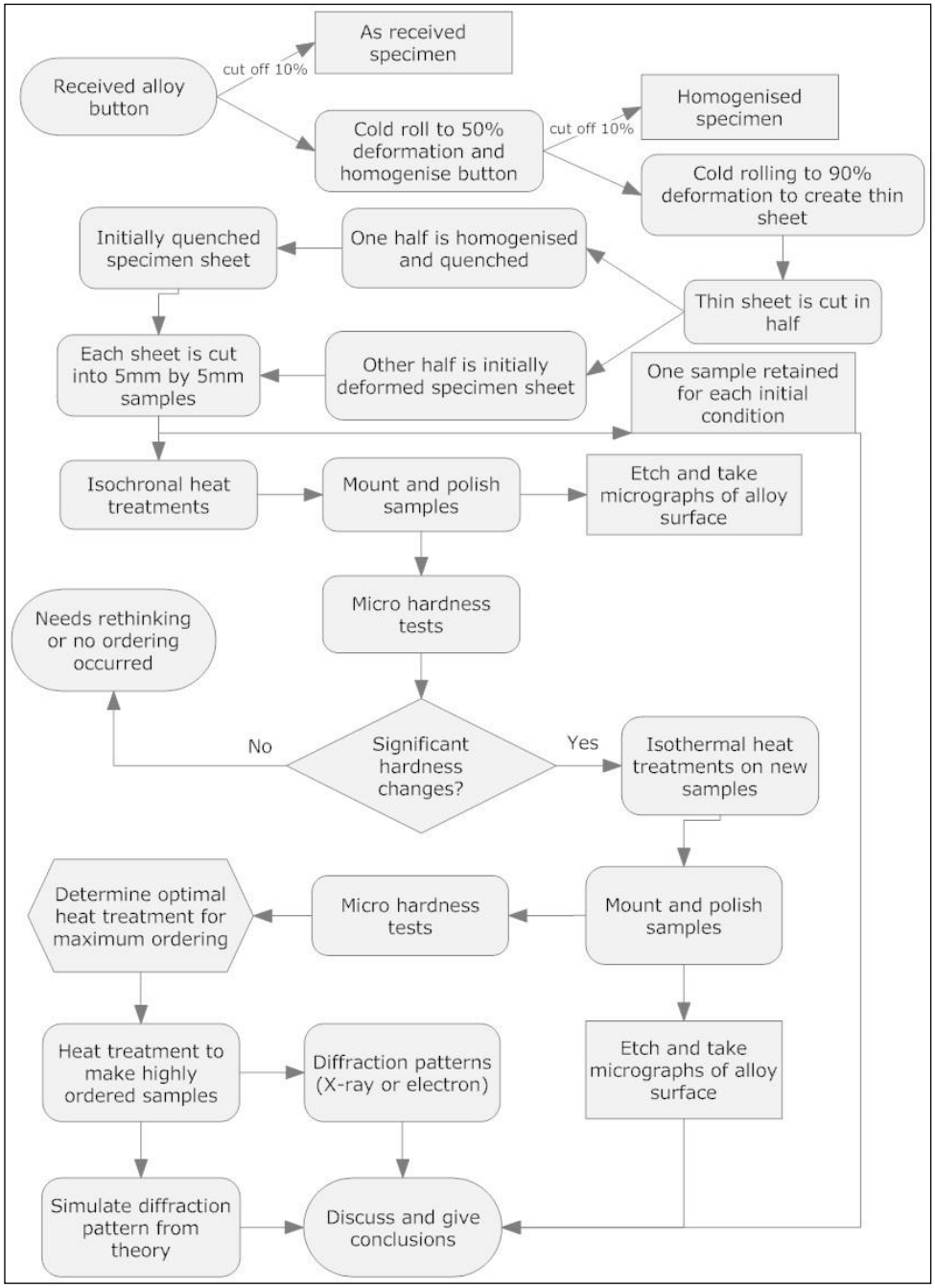

Figure 3.1: Method flow chart

3.1. Homogenisation

The alloy buttons were deformed by 50% using cold rolling and then homogenised at 70% °C of the alloys melting temperature for a specific composition. The heat treatment conditions were accordingly 1000 °C for 12 hours for Pd 11.1 at% Cu and 1200 °C for one week for Pd 11.1 at% Nb in the vacuum furnace in an argon atmosphere. The Pd 11.1 at.% Nb alloy required the longer and higher temperature homogenisation heat treatment as its kinetics are very slow in comparison with the Pd 11.1 at.% Cu alloy[51]. Table 3.1 was used for selecting the homogenisation treatment for the Pd 11.1 at.% alloy, in which 1200 °C was chosen for a one week heat treatment. The heat treatment is followed by furnace (slow) cooling. A small piece of the homogenised sample was retained for hardness comparisons.

Table 3.1: Typical equilibration treatments for niobium-palladium alloys (after Giessen *et al*[51])

Temperature (°C)	Time (h)
1900	2
1700	3
1520	4
1450	6
1400	12
1300	48
1200	168 (1 week)
1100	336 (2 weeks)
1000	504 (3 weeks)
900	744 (1 month)
800	1488 (2 months)

3.2. Initial Sample Preparation

The homogenised samples were cut using a Beuhler microslice. The cut samples were then deformed by 90% using cold rolling to create thin sheets of the samples. The thin sheets were cut into approximately 1 cm by 1 cm squares. Some of the Pd-Cu samples are kept in this condition with one being retained for comparison later with the heat treated samples. These samples were known as the 'initially cold worked' samples. The same procedure is applied to the Pd-Nb samples.

Some of the other Pd-Cu samples were heat treated in the vacuum furnace in an argon atmosphere, under the homogenising conditions of 1000 °C for twelve hours, and then immediately quenched. These samples were labelled 'initially quenched' with one being retained for comparison later with the heat treated samples. No 'initially quenched' samples were made from the Pd-Nb samples due to the difficult heat treatment requirements.

3.3. Heat Treatments

All heat treatments were ramped up to their temperatures over a two hour period. Isochronal heat treatments of 3 hours each were first carried out, followed by quenching in room temperature water. Samples were either heat treated in a vacuum or ambient environment; the ambient environment samples were coated with ISOMOL 100 ceramic powder to minimise oxidation. Micro-hardness tests were then carried out. If the hardness results from those heat treatments showed abnormalities such as an unexpected increase or decrease in hardness, then longer isothermal heat treatments were carried out at the temperatures that gave the abnormal hardness results.

3.3.1. Isochronal Heat Treatment

The heat treatment temperatures ranged from 100 °C to 900 °C in 100 °C increments for the Pd-Cu samples, while for the Pd-Nb samples, heat treatments ranged from 300 °C to 900 °C in increments of 100 °C. A low heating rate for each temperature, shown in Table 3.2 (starting from room temperature of 20 °C) was used to prevent an excessive thermal gradient in the material. Each sample was soaked for 3 hours at the required temperature. After the heat treatment was completed, the sample was quenched into room temperature water.

Table 3.2: Heating rate for each isochronal heat treatment

Heat Treatment (°C)	Heating Rate (°C / Min)
100	0.7
200	1.5
300	2.3
400	3.2
500	4.0
600	4.8
700	5.7
800	6.5
900	7.3

3.3.2. Isothermal Heat Treatment

Heat treatment temperatures which gave significant hardness changes in the isochronal heat treatment were selected for isothermal heat treatments ranging from 3 hours to 48 hours. Once each heat treatment was complete, the sample was quenched into room temperature water.

3.4. Polishing

The samples were first mounted into a resin (epoxy resin for cold mounting and Struers ClaroFast resin for hot mounting). The epoxy resin was used for very thin samples to provide better edge retention and create oblique sections, but if the sample was over 0.5mm thick then hot mounting with ClaroFast was used instead as it takes less time to cure the resin (making oblique samples can take up to 16 hours while hot mounting takes 20 minutes). The samples were ground using 1200 and 2400 grit paper to create a flat surface. The samples were cleaned using ethanol and put into a beaker containing ethanol. The beaker was put into an ultrasonic bath for 5 minutes to loosen any foreign or loose particles on the surface of the samples. The beaker was removed from the ultrasonic bath and the samples taken out and dried using a heat dryer. The samples were then polished using polishing pads designed to use diamond paste of differing particle sizes starting with 6μm then 3μm, 1μm and finally 0.25μm. Each sample was polished for 1 to 5 minutes with each successive step having a longer polish time that the previous step. Between each polish, the samples were cleaned using ethanol (or methanol) and put into the ultrasonic bath as after the grinding step.

3.5. Microhardness Tests

Once the samples had gone through the necessary heat treatments and mounting, microhardness was tested using an Indentec model HWDM-3 microhardness tester; using a Vickers indenter under 100 grams force. Ten microhardness readings are collected for each sample. The readings are plotted using Microsoft Excel.

3.6. Etching

The solution used to etch the Pd 11.1 at% Cu samples was a mixture of 4 grams $Cr0_3$ and 50ml of HCl. The etching solution was dropped onto the sample surface using a dropper, and allowed to etch for 1 minute. After etching, the samples were immediately cleaned with distilled water.

The solution used to etch the Pd 11.1 at% Nb samples was a mixture of 20g ammonium persulphate in 90ml of distilled water (solution A) and 20g potassium cyanide in 90ml of distilled water (solution B). Solution A and solution B were mixed in equal parts and the resulting mixture was poured onto the sample surface, in a fume hood, with a plastic dropper and allowed to etch for three minutes until a visible change was observed on the surface; the samples were then rinsed with distilled water to remove the etchant.

3.7. Differential Scanning Calorimetry (DSC)

For DSC, small discs were made from the Pd 11.1 at.% Nb alloy and were ground until roughly 20mg in weight, making sure the weight does not drop below 20mg. DSC is a thermalanalytical technique that measures the amount of heat required to increase the temperature of a sample and reference material as a function of temperature. DSC is commonly used to detect phase transitions, as the sample undergoes a physical transition that will require more or less heat to flow than the reference to maintain both at the same temperature, depending on whether the process is exothermic or endothermic in nature. A *Netzsch STA409* thermal analyser was used, fitted with an S-type thermocouple.

3.8. Scanning Electron Microscopy (SEM)

For SEM, samples were mounted in resin or attached to a metal stub. Samples were made electrically conductive by either coating the surface of the sample with an electrically conductive element or by using silver dag to complete the electric circuit in the SEM sample holder. SEM was used to: acquire images of the sample surface at a higher resolution than light microscopy, determine composition using Energy Dispersive Spectroscopy (EDS), or capture an image showing atomic number contrast using a backscatter detector. This allowed for an investigation into compositional variations in the sample over features present on the surface. A *FEI Nova™ NanoSEM 230* scanning electron microscope (SEM) was used with a 20 kV accelerating voltage.

3.9. Transmission Electron Microscopy (TEM)

Samples were made from the initially deformed material (approximately 80% to 90% deformed), by punching out 3mm diameter disks from the metal alloy sheet. The TEM disks were heat treated and quenched in room temperature water. The heat treated TEM disks were ground (using 1200 grit silicon carbide paper) to a thickness of less than or equal to 100 microns, measured with a micrometre. The sample disks were then ground with a 6 micron diamond paste using the Gatan dimpler. Continuing with the Gatan dimpler the disks were polished with 3 micron diamond paste, 1 micron diamond paste and lastly a 0.25 micron diamond paste, while making sure to use different polishing pads and keeping contamination to a minimum.

The final process is to use the Gatan Precision Ion Polishing System to create electron transparent samples. Polishing is carried out with an ion beam, with a starting angle of 6 degrees, followed by 3 degrees. Once a hole is formed, the sample is ready for TEM. The TEM discs were used in a *Philips TECNAI TF20* electron microscope, equipped with a Field Emission Gun (FEG) for diffraction patterns and a FEI TECNAI T20 TEM for imaging and Electron Spectroscopic Imaging (ESI). ESI makes use of an energy filter (in this case, a Gatan Image Filter, GIF) to record the Electron Energy Loss Spectra (EELS) which is mapped to a TEM image. EELS measures the inelastic scattering of electrons, and by using a known, narrow range of kinetic energy the energy loss can be measured and characterized for the cause of the energy loss.

Diffraction patterns were digitally recorded at selected zone axes. The electron transparent region of the TEM disk was captured digitally in selected areas, and these selected areas also underwent spectrographic analysis using ESI. The resulting images were digitally recorded.

4. Results

This chapter presents results obtained from microhardness testing, light microscopy, scanning electron microscopy, simulated diffraction patterns and transmission electron microscopy.

4.1. Palladium-copper

This section contains results for the palladium 11.1 atomic % copper alloy.

4.1.1. Microhardness Measurements

Figure 4.1 below shows the average microhardness of initially cold worked (90%) samples of Pd 11.1 at% Cu after heat treatments for 3 hours, with the as-received, homogenised and deformed conditions added for comparison. The initially cold worked (deformed) samples that underwent heat treatments at 100 °C, 200 °C and 300 °C for 3 hours each respectively showed no significant average microhardness changes, relative to the deformed sample. However, the sample heat treated at 300 °C for 3 hours does have the highest average microhardness relative to the other samples. For the samples heat treated at 400 °C, 500 °C and 600 °C for 3 hours each respectively, a decreasing trend is noted for the average microhardness relative to the deformed sample. Also the sample heat treated at 600 °C for 3 hours showing a large standard deviation relative to the other samples. The samples heat treated at 700 °C, 800 °C and 900 °C for 3 hours each respectively all have a low average microhardness relative to the deformed sample, and are comparable to the average microhardness of the homogenised sample.

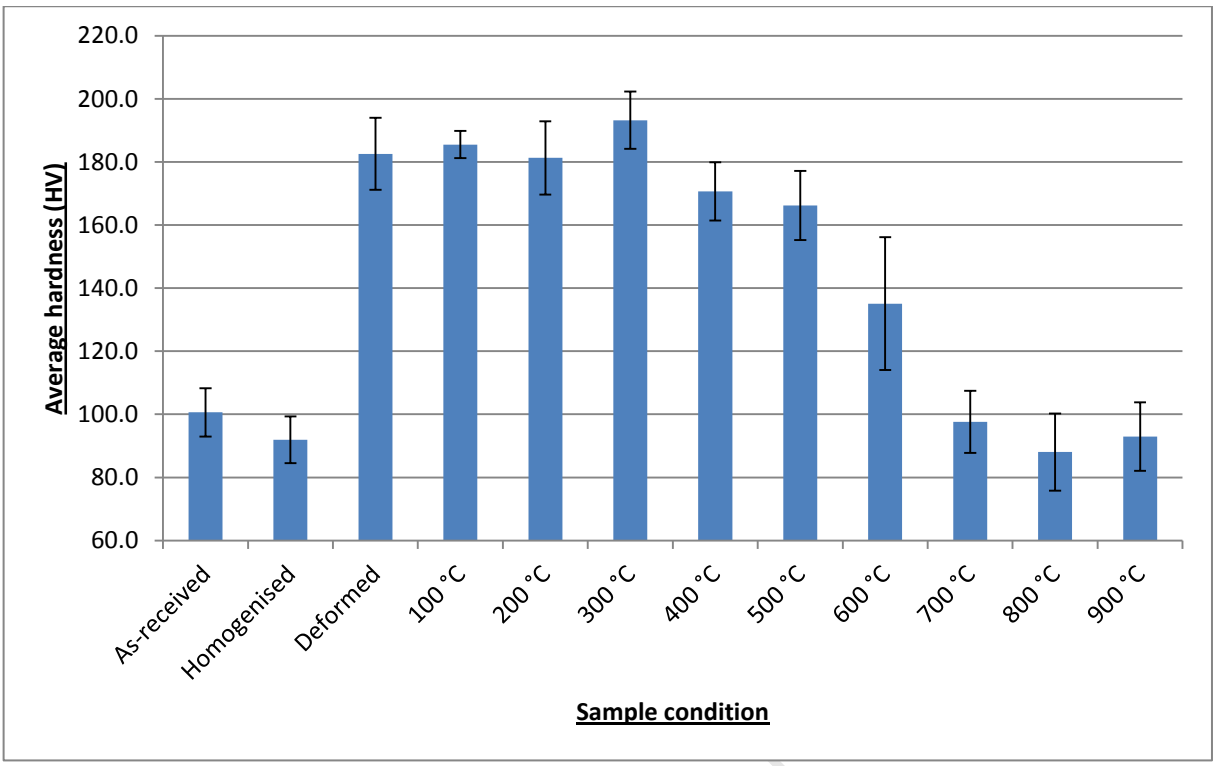

Figure 4.1: Average microhardness measurements of selected initially cold worked Pd 11.1 at% Cu samples after heat treatments of 3 hours

Figure 4.2 shows the hardness of the initially quenched samples of Pd 11.1 at% Cu, before and after heat treatment at 300 °C and 600 °C for 3 hours each respectively. The heat treated samples did not show a significant increase in microhardness relative to the quenched sample when the overlap in error bars is considered. For the 900 °C for 3 hours initially quenched sample the average microhardness showed a decrease relative to the sample before heat treatment. For the initially quenched condition it was surmised that no significant microhardness changes would be seen on the basis of the results on Figure 4.2.

Figure 4.3 shows the results of microhardness measurements on isothermal heat treatments of a new set of initially deformed samples, at 300 °C for 3 hours, 6 hours, 12 hours, 24 hours and 48 hours respectively. A heat treatment temperature of 300 °C was selected, as it was the highest temperature that gave the highest average microhardness in Figure 4.1. The average microhardness values of the deformed, 3 hours and 6 hours samples are seen to be similar with their error bars overlapping. The 12 hours, 24 hours and 48 hours samples respectively have a lower average microhardness value relative to the deformed sample and the 6 hours sample but are seen to be similar to each other with their error bars overlapping significantly.

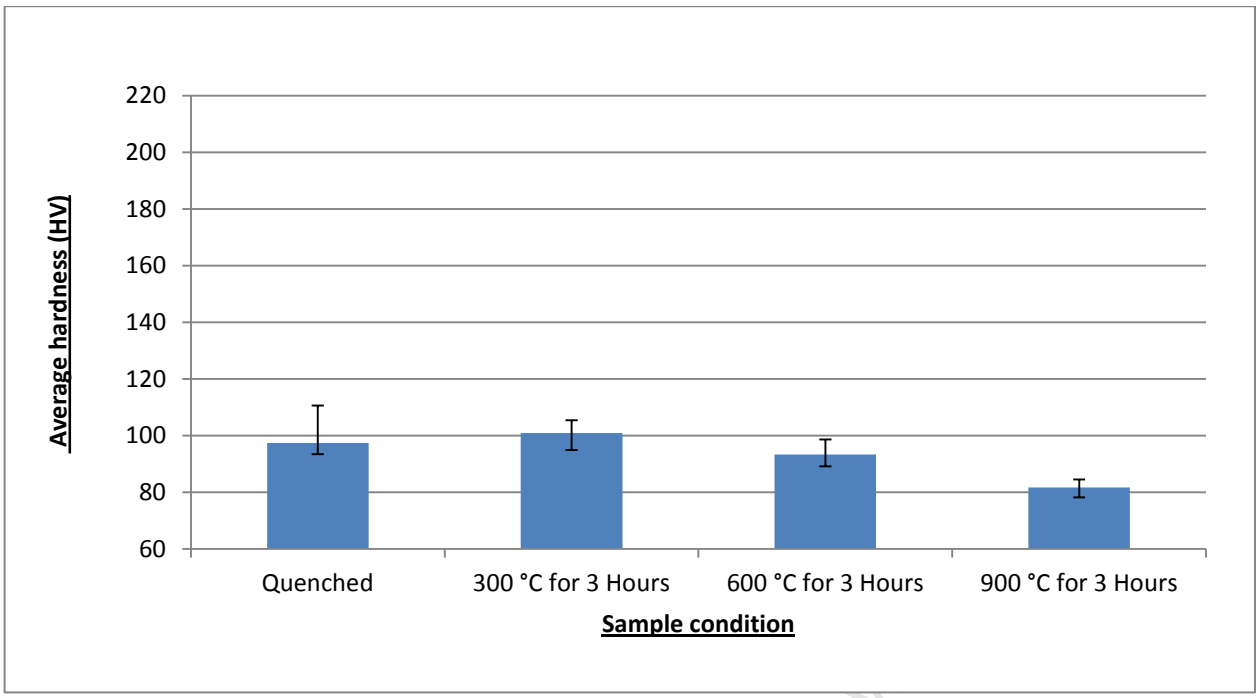

Figure 4.2: Average microhardness measurements of initially quenched Pd-11.1 at% Cu samples after 3 hour heat treatments.

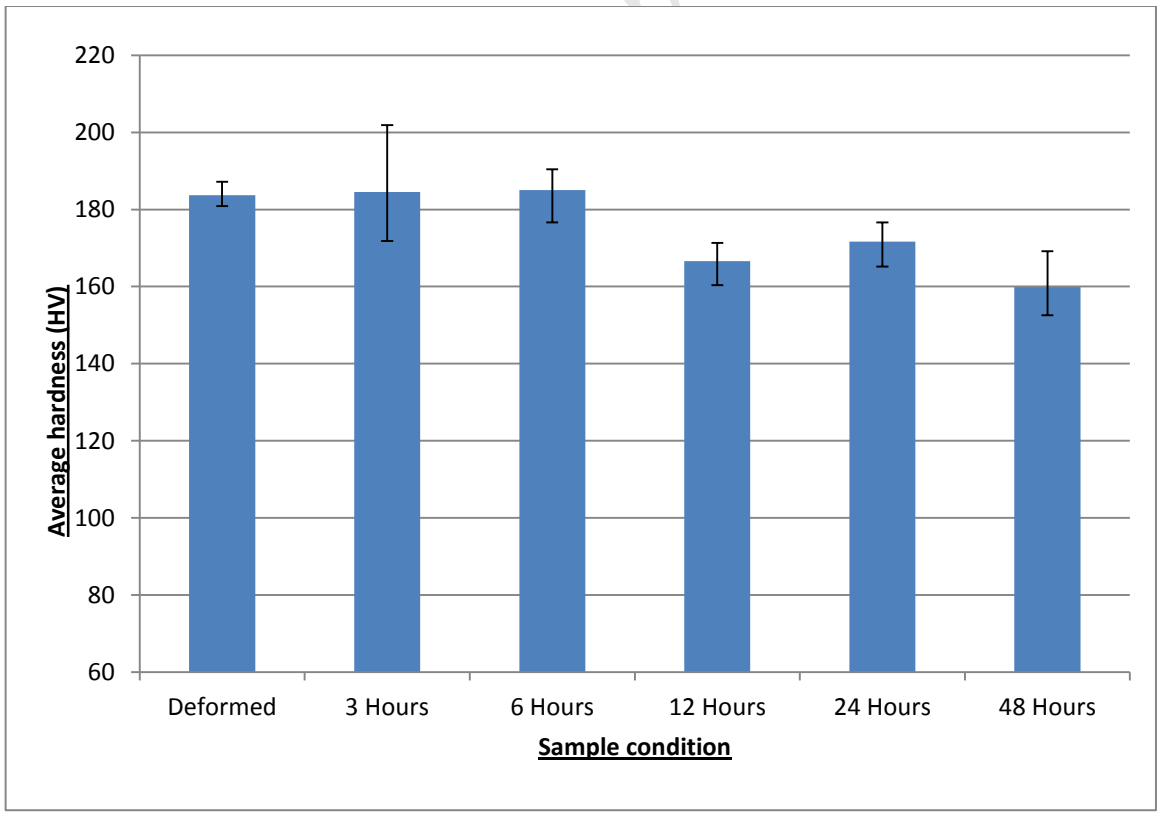

Figure 4.3: Average microhardness measurements of initially cold worked Pd 11.1 at% Cu samples after isothermal 300 °C heat treatments.

4.1.2. Light microscopy

This section shows the light microscopy micrographs taken of the initially cold worked (deformed) samples. The homogenised sample (heat treated at 1200 °C for 12 hours) in Figure 4.4 shows an equiaxed grain structure. Figure 4.5 shows the ~90% deformed sample before heat treatment, and shows grains elongated in the rolling direction. The sample heat treated at 300 °C for 3 hours, as shown Figure 4.6, retains the elongated grains from the ~90% deformation condition.

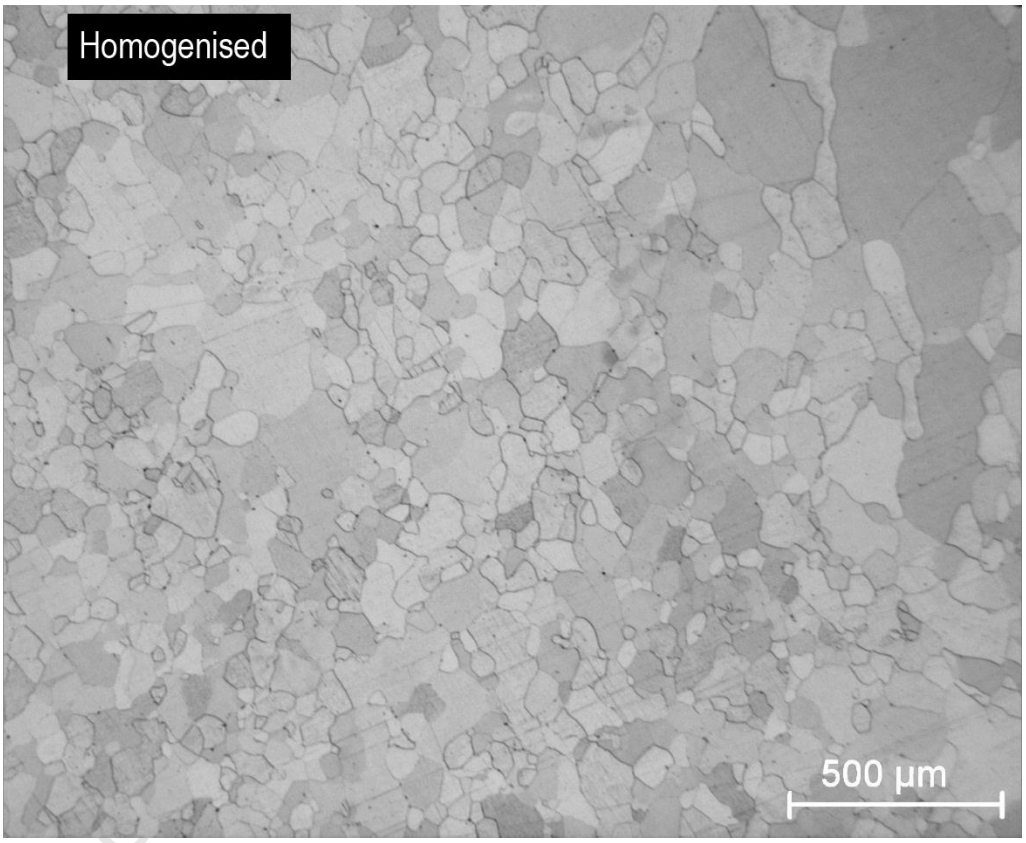

Figure 4.4: Micrograph of homogenised Pd-Cu alloy.

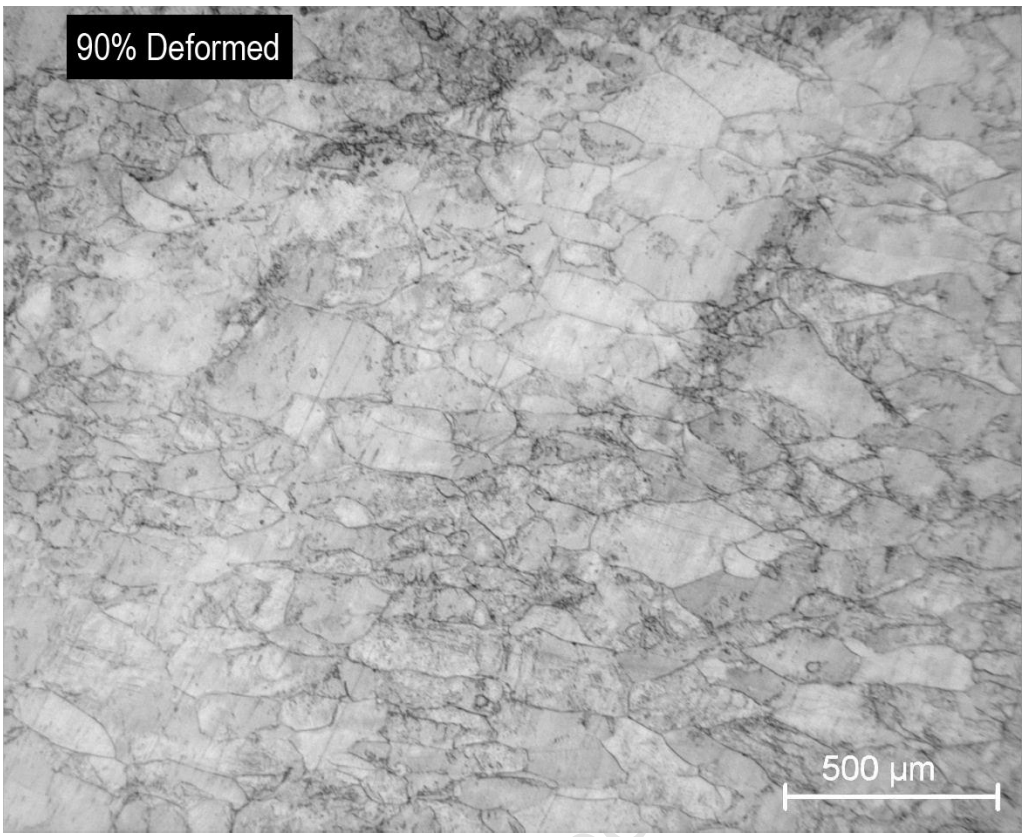

Figure 4.5: Micrograph of Pd-Cu alloy after 90% deformation prior to heat treatments

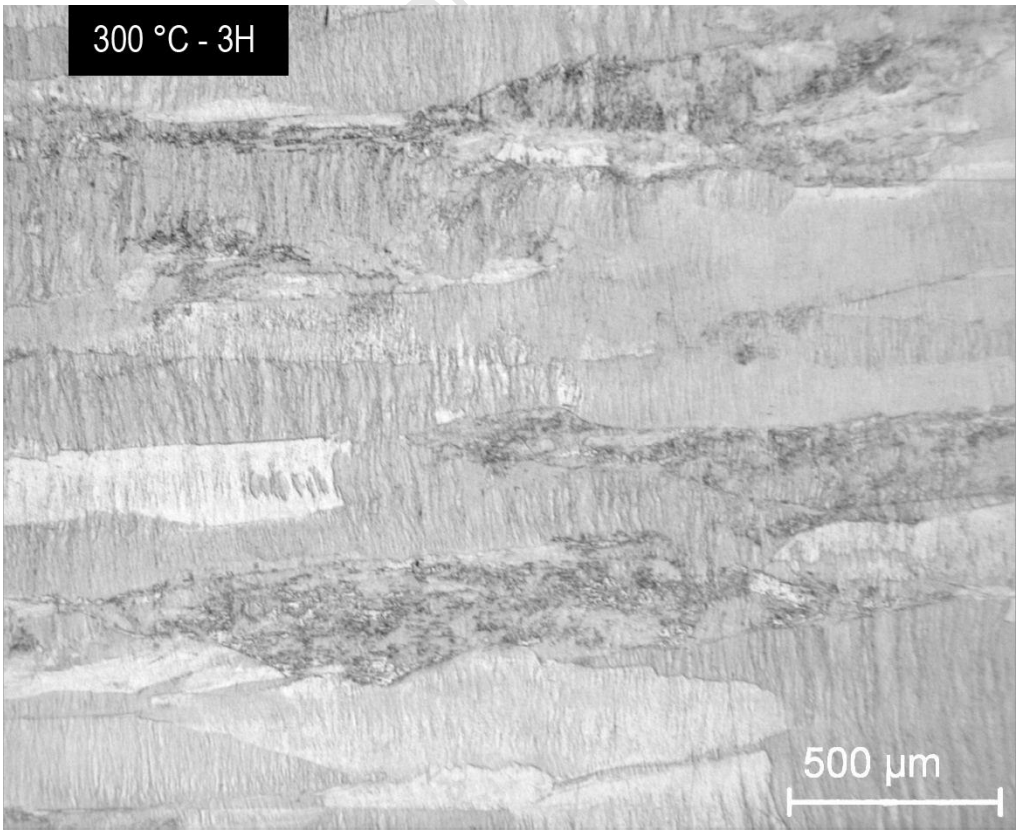

Figure 4.6: Micrograph of Pd-Cu alloy after heat treatment at 300 °C for 3 hours

The sample heat treated at 400 °C for 3 hours in Figure 4.7 has similar features to the sample heat treated at 300 °C for 3 hours. The sample heat treated at 700 °C for 3 hours in Figure 4.8 has lost the elongated grains and shows a refined grain structure, and appears to be recrystallized. The sample heat treated at 900 °C for 3 hours in Figure 4.9 is similar to the sample heat treated at 700 °C for 3 hours and also shows the recrystallized condition.

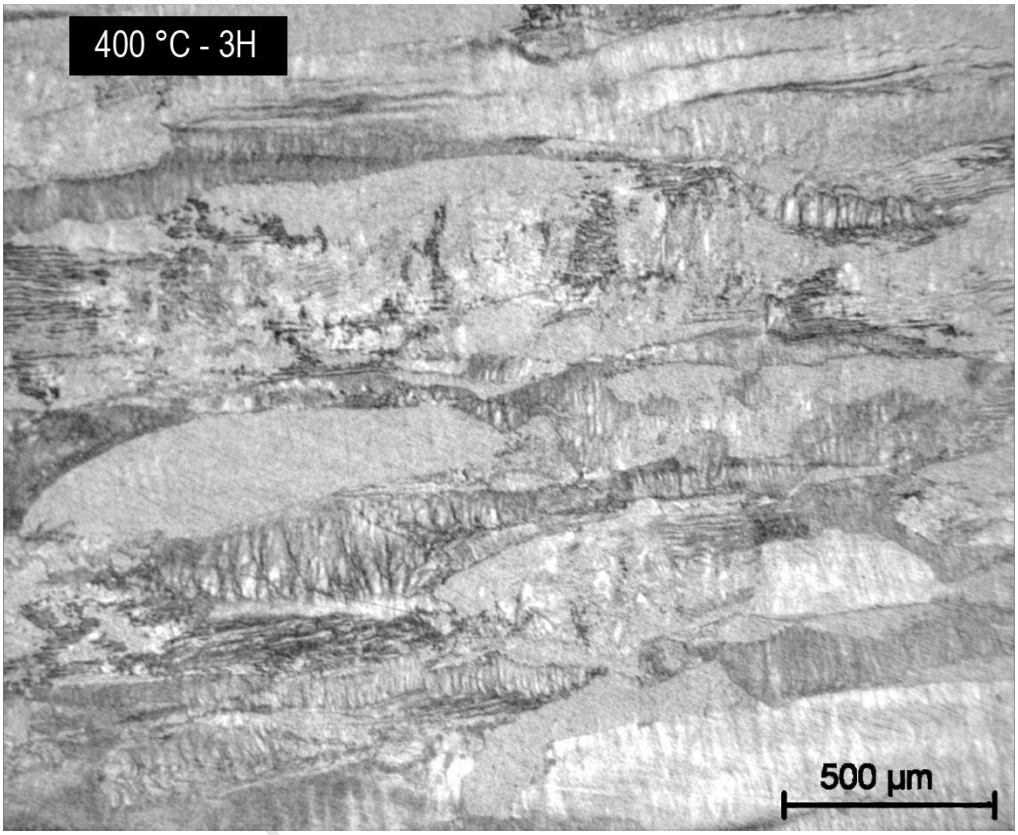

Figure 4.7: Micrograph of Pd-Cu alloy after heat treatment at 400 °C for 3 hours.

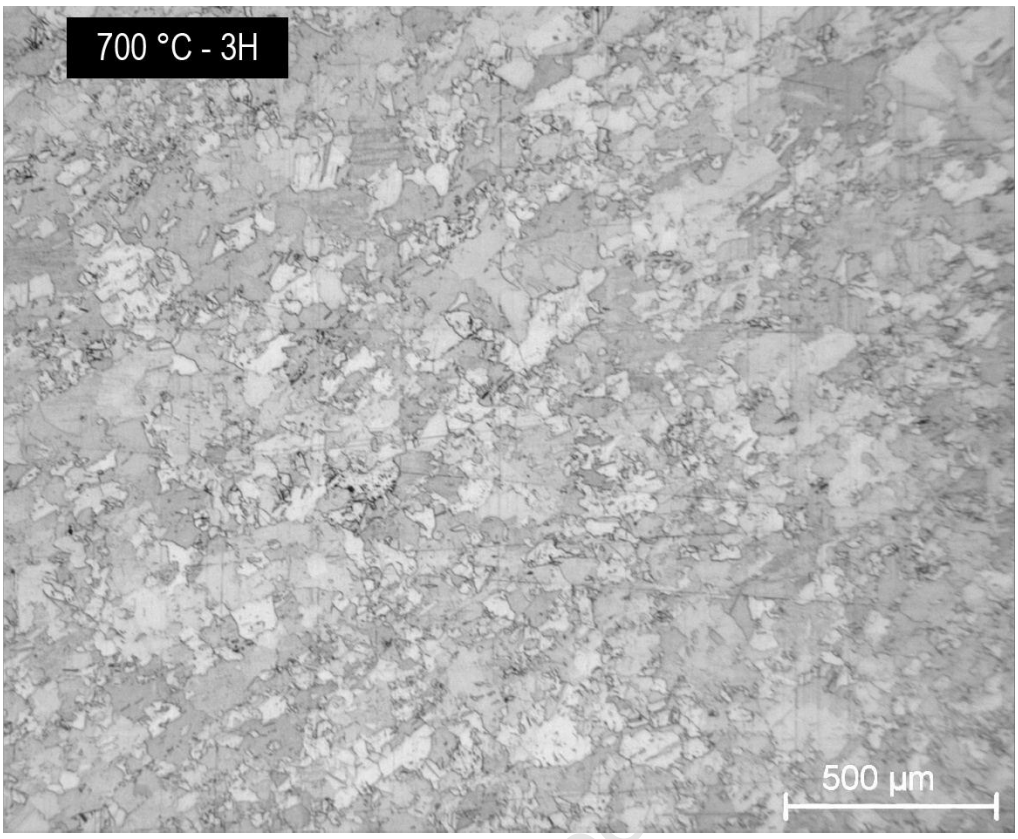

Figure 4.8: Micrograph of Pd-Cu alloy after heat treatment at 700 °C for 3 hours.

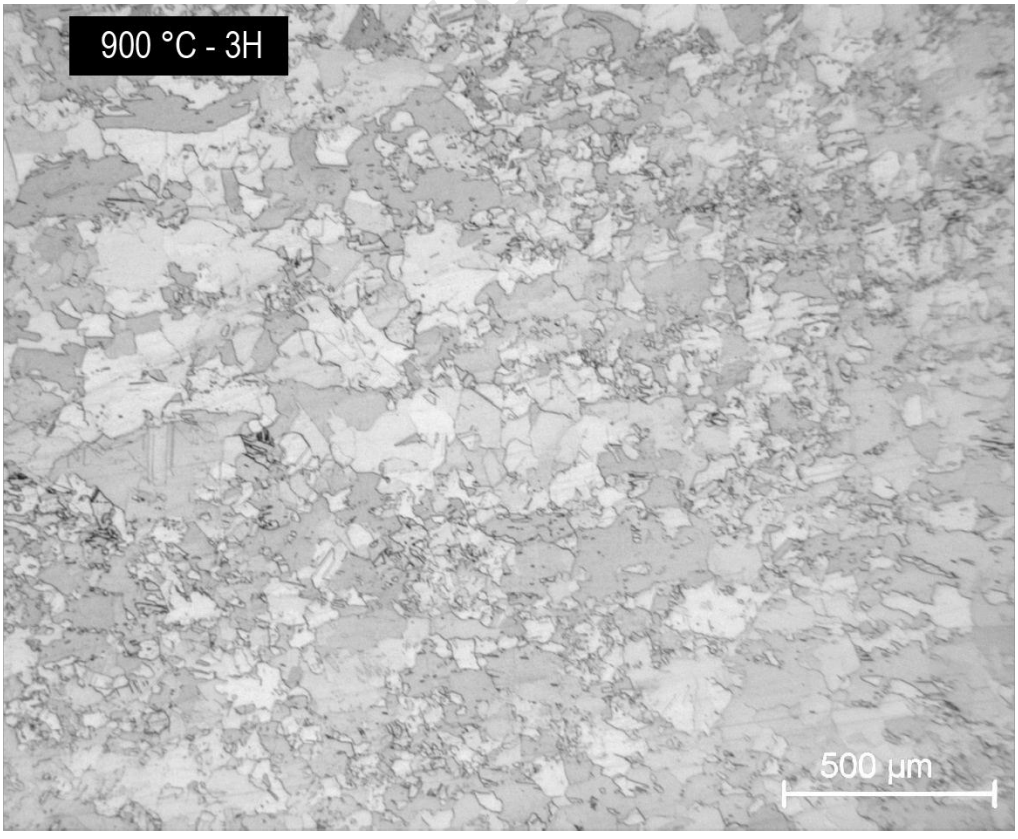

Figure 4.9: Micrograph of Pd-Cu alloy after heat treatment at 900 °C for 3 hours.

Figure 4.10, Figure 4.11 and Figure 4.12 show heat treated Pd 11.1 at.% Cu at 300 °C for 12 hours, 24 hours and 48 hours respectively. When compared with the sample heat treated at 300 °C for 3 hours (Figure 4.6) they still have the elongated grains with very little change to the microstructure.

Figure 4.10: Micrograph of Pd-Cu alloy after heat treatment at 300 °C for 12 hours.

Figure 4.11: Micrograph of Pd-Cu alloy after heat treatment at 300 °C for 24 hours.

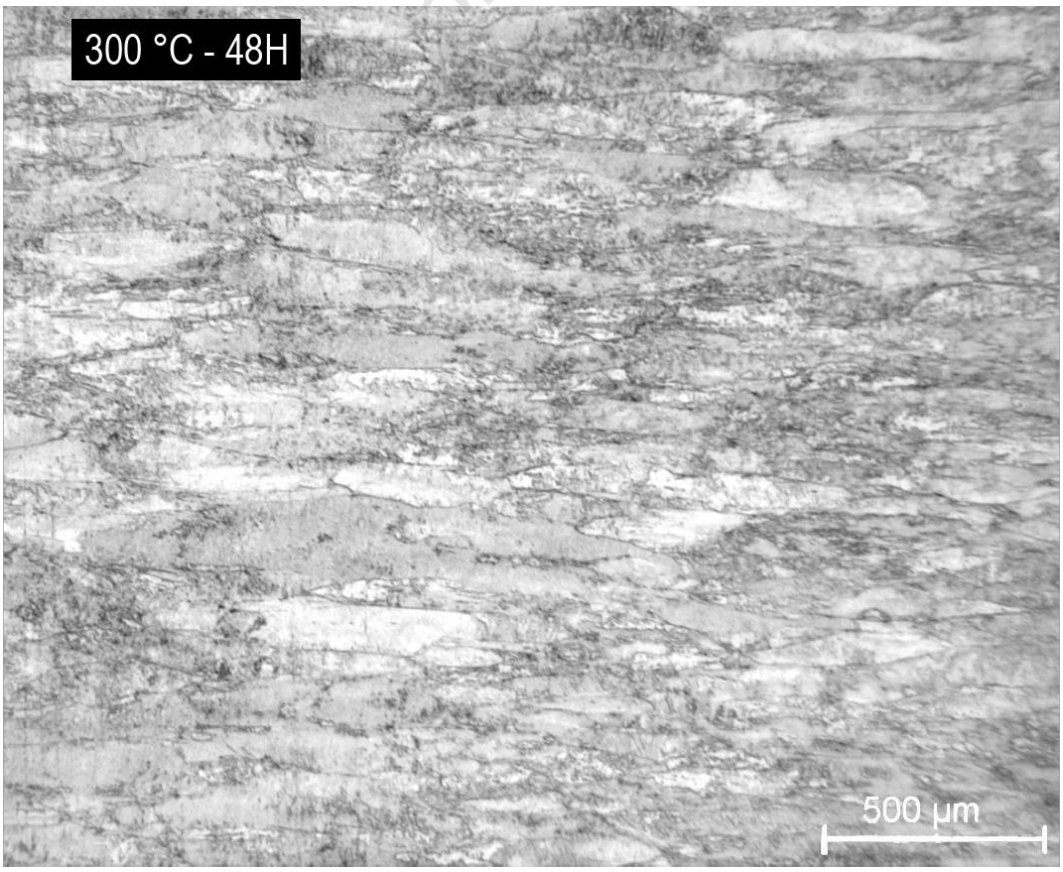

Figure 4.12: Micrograph of Pd-Cu alloy after heat treatment at 300 °C for 48 hours.

4.1.3. SEM/EDS

SEM was used to measure the homogenised alloy composition. The results for the EDS are shown in Table 4.1 below. Two random areas were chosen and area maps were taken. Spectrographs of the EDS data are also shown below in Figure 4.13 and Figure 4.14 for Area 1 and Area 2 respectively. The EDS data shows good homogeneity for the sample, with the expected composition of palladium 11.1 at.% copper.

Table 4.1: EDS data for the heat treated at 1000 °C for 12 hours Pd-Cu sample

	Area 1	Area 2	% Error
Weight percentage Pd	93.04	93.32	~1%
Weight percentage Cu	6.96	6.68	~1%
Atomic percentage Pd	88.87	89.30	~1%
Atomic percentage Cu	11.13	10.70	~1%

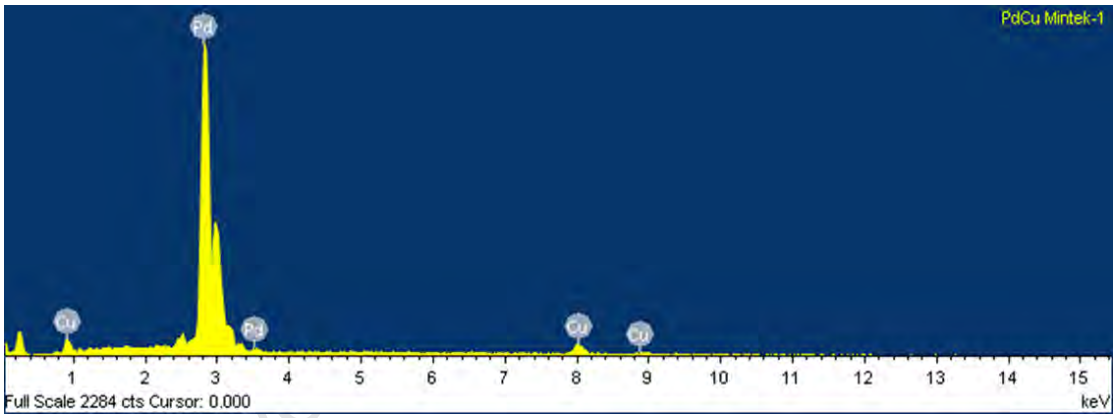

Figure 4.13: EDS spectrograph of Area 1

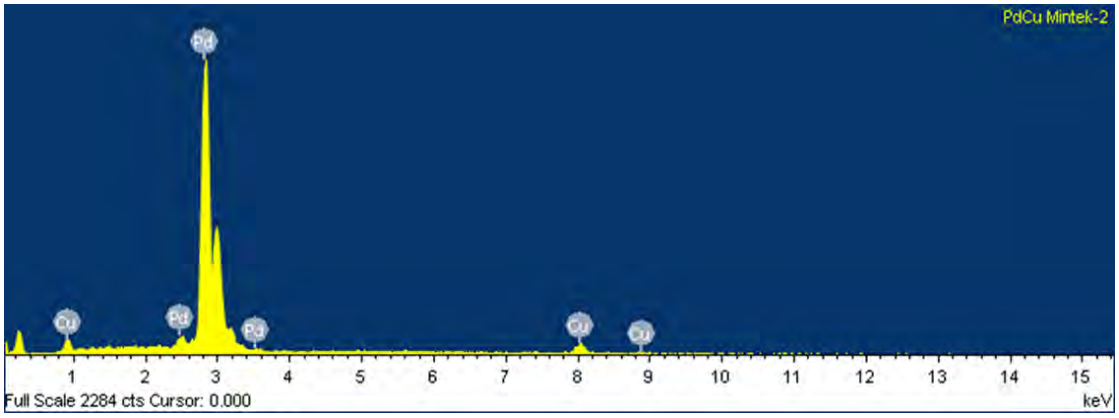

Figure 4.14: EDS spectrograph of Area 2.

SEM EDS was carried out on the samples heat treated at 200 °C for 3 hours, 300 °C for 3 hours, 400 °C for 3 hours and 700 °C for 3 hours. Figure 4.15 and Figure 4.16 illustrates the method used in SEM for EDS analysis of the sample heat treated at 300 °C for 3 hours. For Figure 4.15 spectrum 1 is an area EDS analysis, while spectrums 2 to 6 are spot EDS analyses, with their results tabulated in Table 4.2.

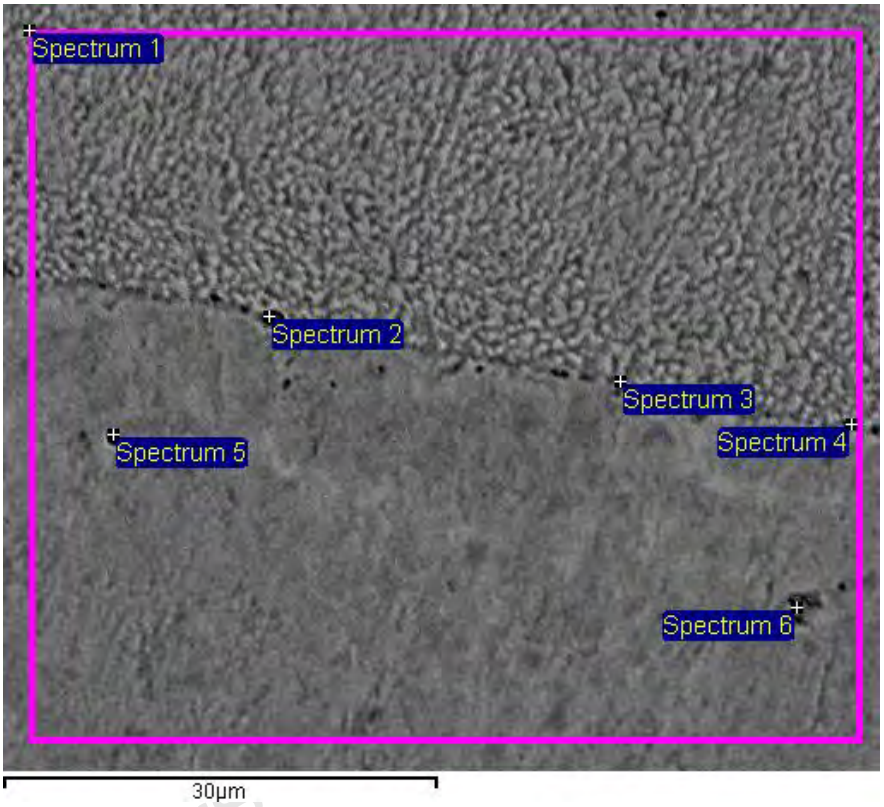

Figure 4.15: SEM backscatter image of Pd 11 at.% Cu heat treated at 300 °C for 3 hours showing EDS analysis locations.

Table 4.2: SEM EDS analysis on Pd 11.1 at.% Cu heat treated at 300 °C for 3 hours sample

Spectrum	Cu atomic percentage(at.%)	Pd atomic percentage (at.%)
Spectrum 1	10.25	89.75
Spectrum 2	11.83	88.17
Spectrum 3	12.69	87.31
Spectrum 4	11.87	88.13
Spectrum 5	11.16	88.84
Spectrum 6	12.37	87.63
Mean	11.69	88.31
Std. deviation	0.88	0.88

In some cases an EDS line spectrum was done, such as the case of Figure 4.16 and Figure 4.17 for the sample heat treated at 300 °C for 3 hours. This was used to investigate grain boundaries and any artefacts seen in the backscatter images of the samples investigated at SEM. The selected results of the line spectrums are tabulated in Table 4.3, and show no significant compositional changes in atomic copper percentage.

Figure 4.16: SEM backscatter image of Pd 11 at.% Cu heat treated at 300 °C for 3 hours showing EDS analysis using line spectrums.

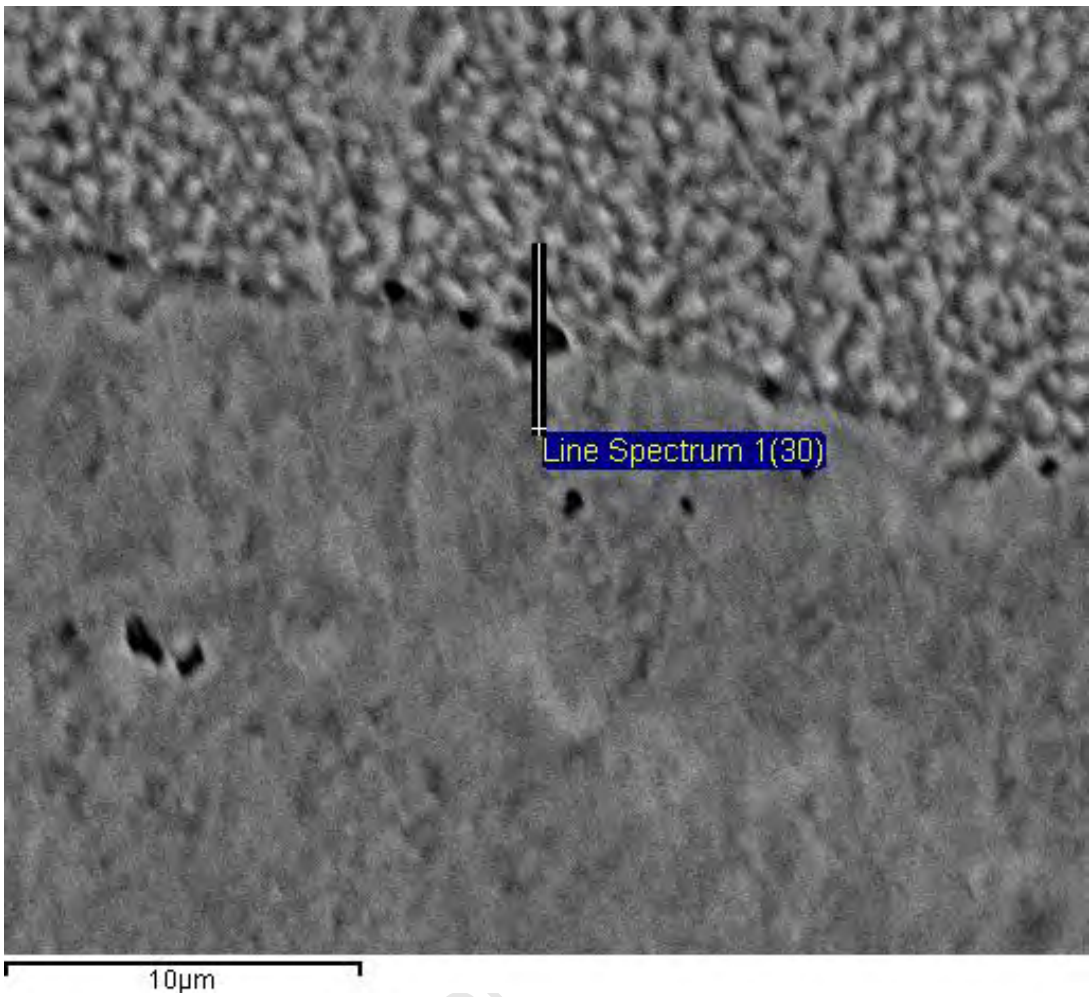

Figure 4.17: SEM backscatter image of Pd 11 at.% Cu heat treated at 300 °C for 3 hours showing EDS analysis of an artefact using line spectrums.

Table 4.3: Selected SEM EDS analysis of Pd 11.1 at.% Cu heat treated at 300 °C for 3 hours

	Average Cu atomic percentage (at.%)	Average Pd atomic percentage (at.%)	Standard Deviation
Figure 4.16			
Line Spectrum 1	10.83	89.17	0.56
Line Spectrum 2	10.88	89.12	0.44
Line Spectrum 3	10.82	89.18	0.42
Figure 4.17			
Line Spectrum 1	12.3	87.7	1.33

A SEM EDS grid of 20 by 20 spots was done on the sample heat treated at 300 °C for 3 hours as shown in Figure 4.18 and Figure 4.19 (on the following page) to investigate the light and dark patterns within the grains, and to see if any compositional variance matched the patterns.

While the grid in Figure 4.19 seems to show some compositional variance with copper, the compositional difference is minor (~2%) and may fall within the measurement error of the SEM, which is roughly 1% to 2%. There also was no clear indication that the compositional variance of copper was following what was noted on the microstructure.

Overall no significant compositional atomic percentage changes were seen on all samples analysed using SEM EDS in backscatter mode.

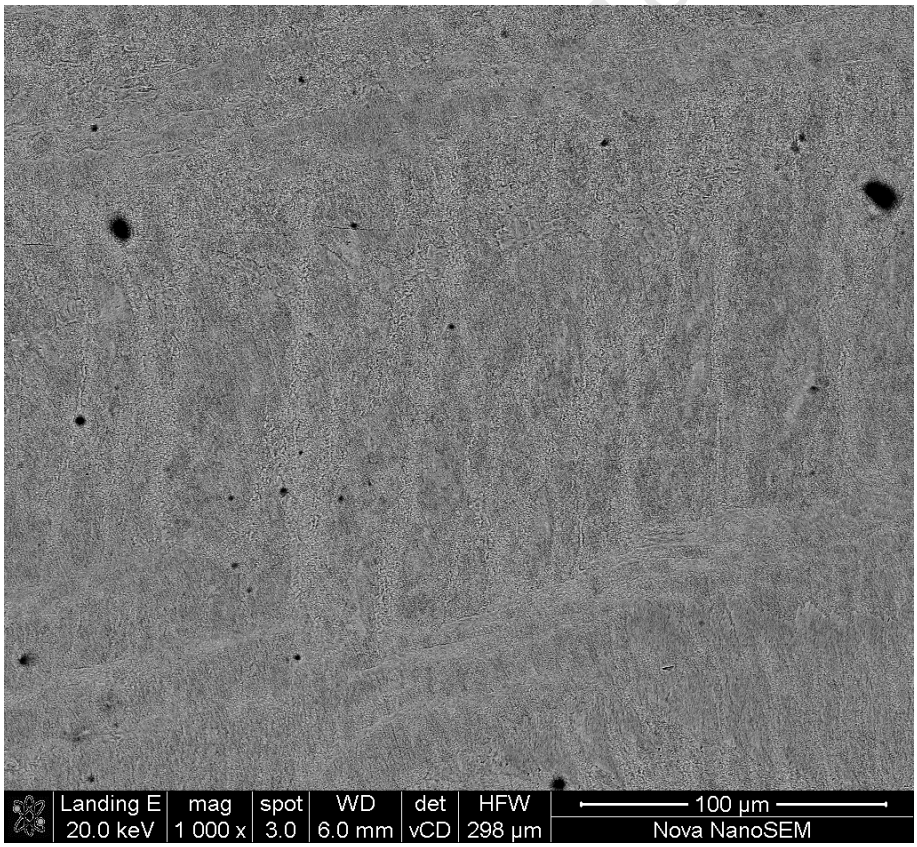

Figure 4.18: SEM backscatter image of Pd 11 at.% Cu heat treated at 300 °C for 3 hours sample.

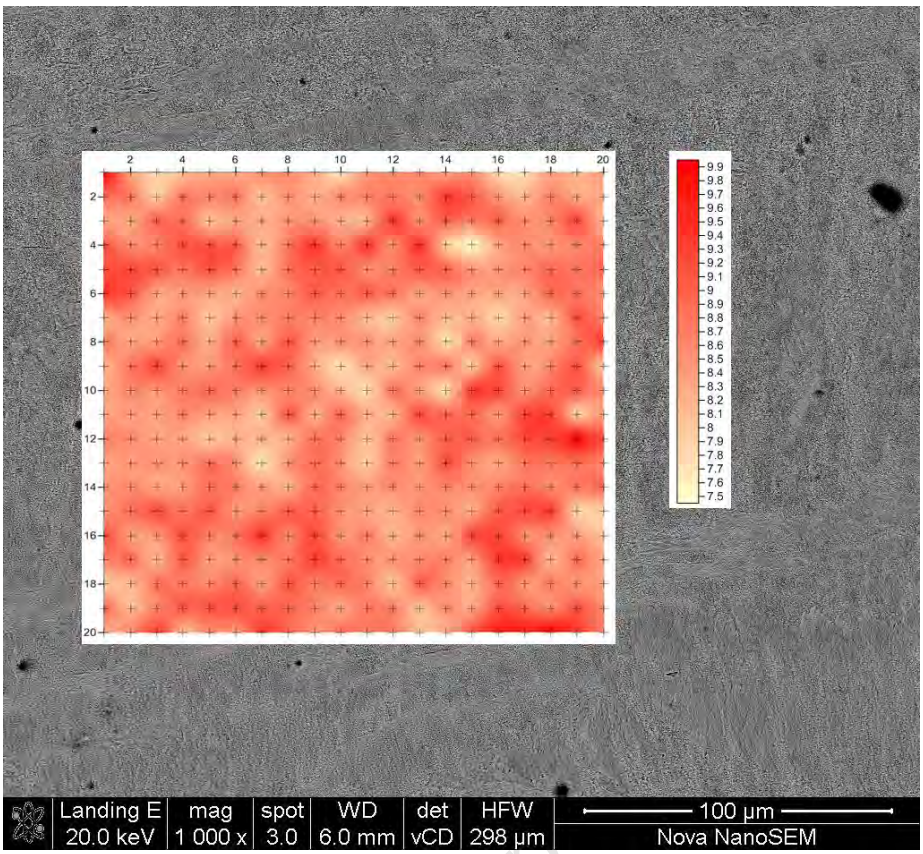

Figure 4.19: SEM EDS grid of Pd 11 at.% Cu heat treated at 300 °C for 3 hours sample (red = increasing copper atomic percent).

4.1.4. TEM Electron Diffraction

TEM analysis was carried out on the Pd-Cu alloy. The deformed (only cold worked) Pd 11.1 at% Cu sample, showed only the fundamental FCC reflections with no extra diffraction spots on the zone axes as shown in Figure 4.20. For the initially deformed sample heat treated at 300 °C for 3 hours, no extra diffraction spots were noted on the zone axes shown in Figure 4.21 when compared with their simulated diffraction patterns for Pd_7Cu. The simulated superlattice structure was created using ISOCIF that was developed by Stokes and Campbell[55]. The crystallographic information was then processed by Zuos and Mabons Web-EMAPS[56] to simulate the diffraction pattern.

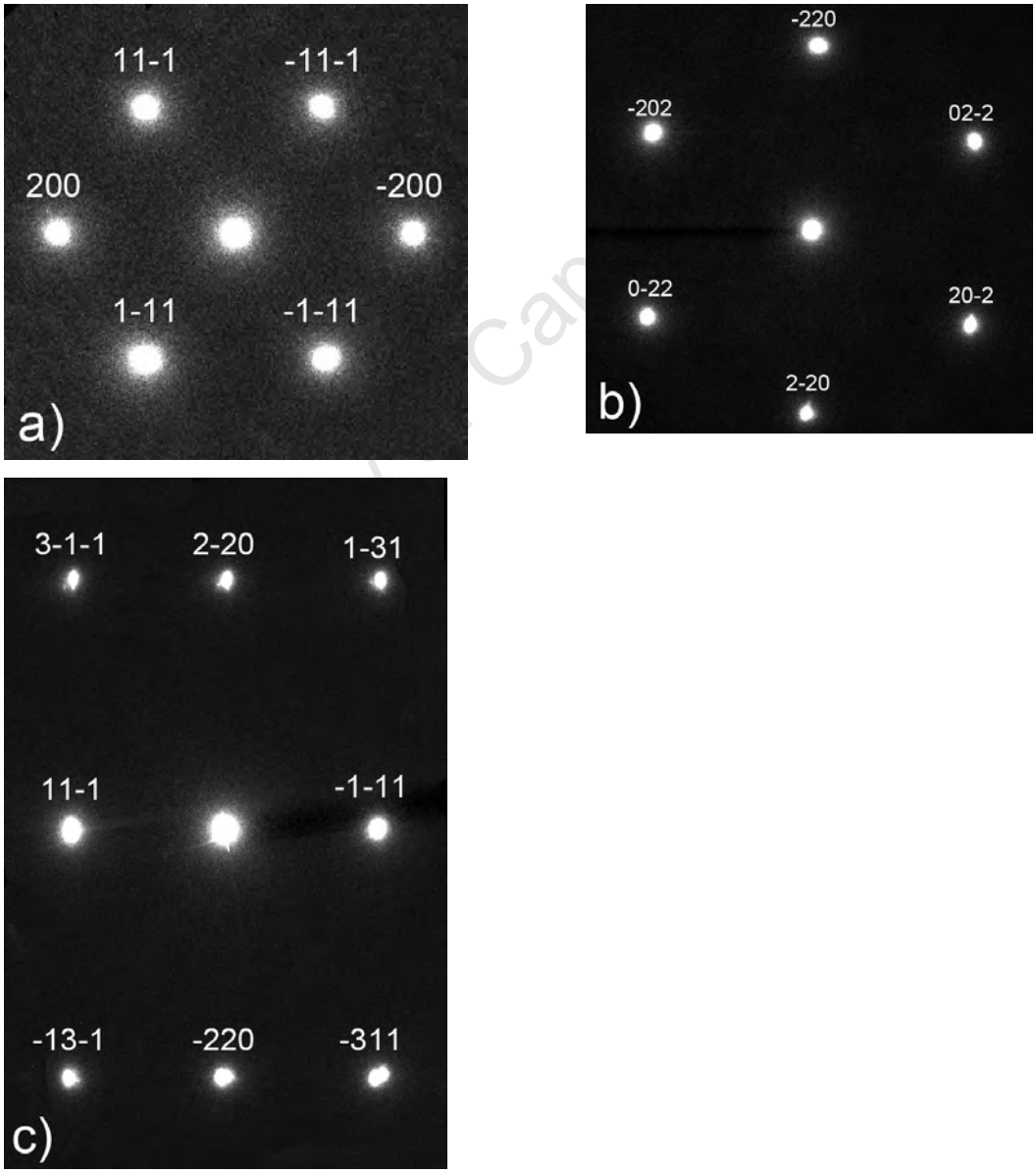

Figure 4.20: TEM experimental diffraction patterns of the deformed sample on zone axes a) [011], b) [111] and c) [112].

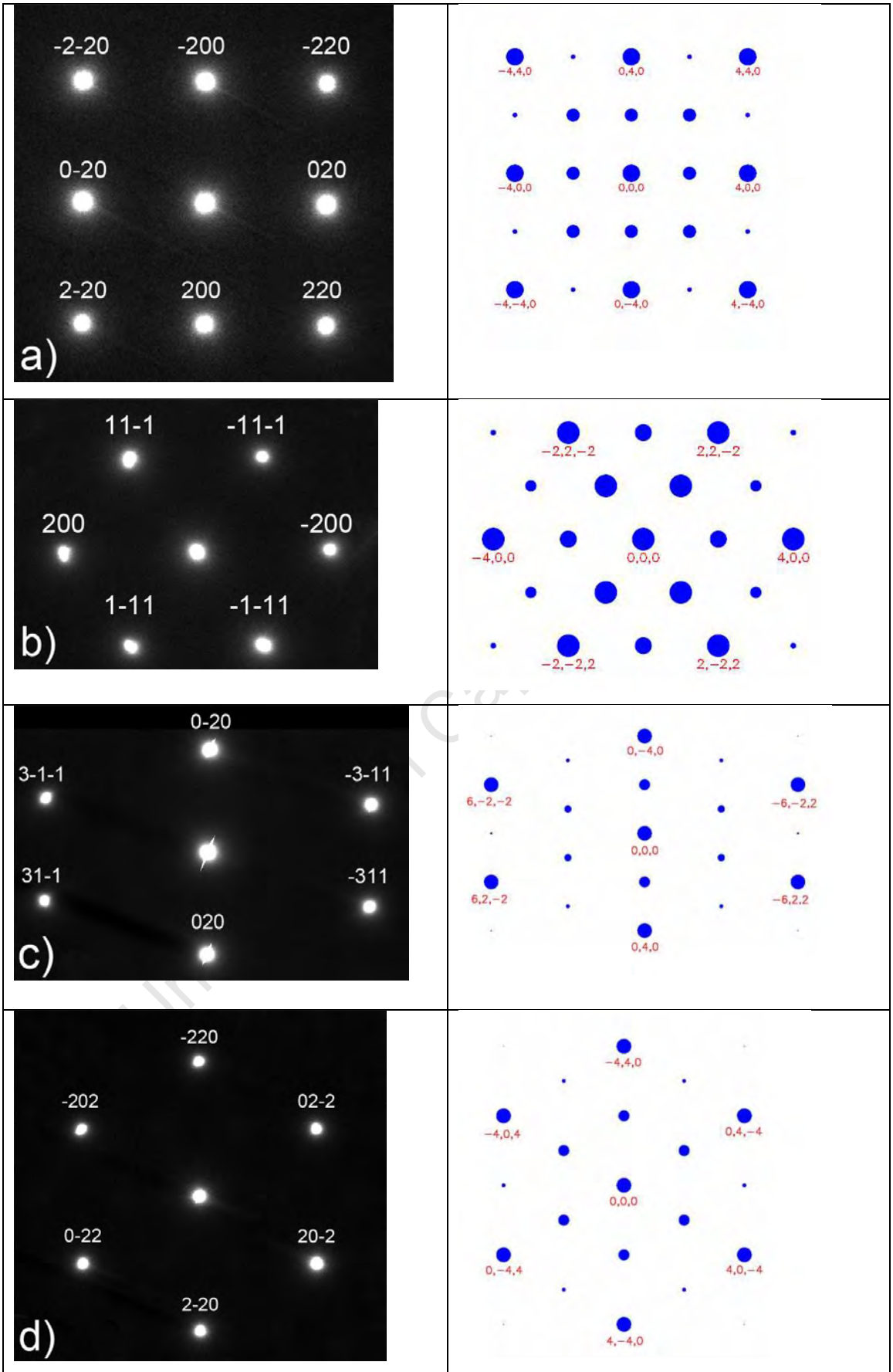

Figure 4.21: TEM experimental diffraction patterns of Pd-Cu alloy after 300 °C for 3 hours, and simulated Pd_7Cu diffraction patterns on zone axes a) [001], b) [011], c) [103], d) [111] and e) [112].

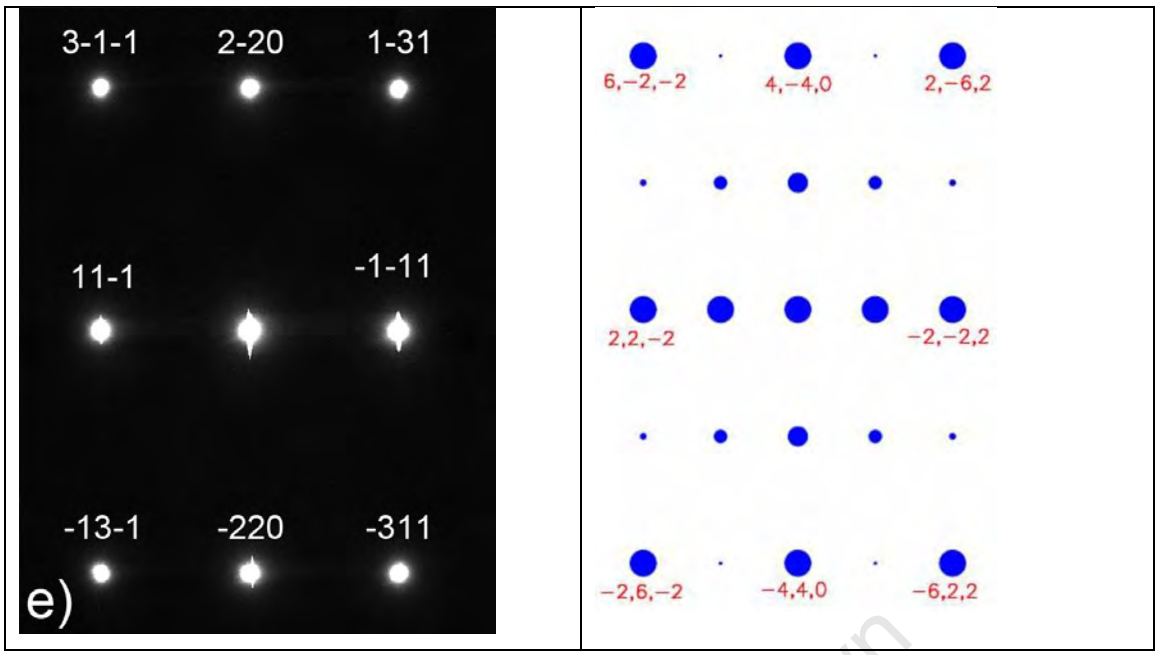

Figure 4.21: TEM experimental diffraction patterns of Pd-Cu alloy after 300 °C for 3 hours, and simulated Pd_7Cu diffraction patterns on zone axes a) [001], b) [011], c) [103], d) [111] and e) [112].

4.1.5. TEM Imaging and ESI

Further analysis was carried out on the Pd-Cu alloy via TEM imaging and using ESI and EELS to map composition.

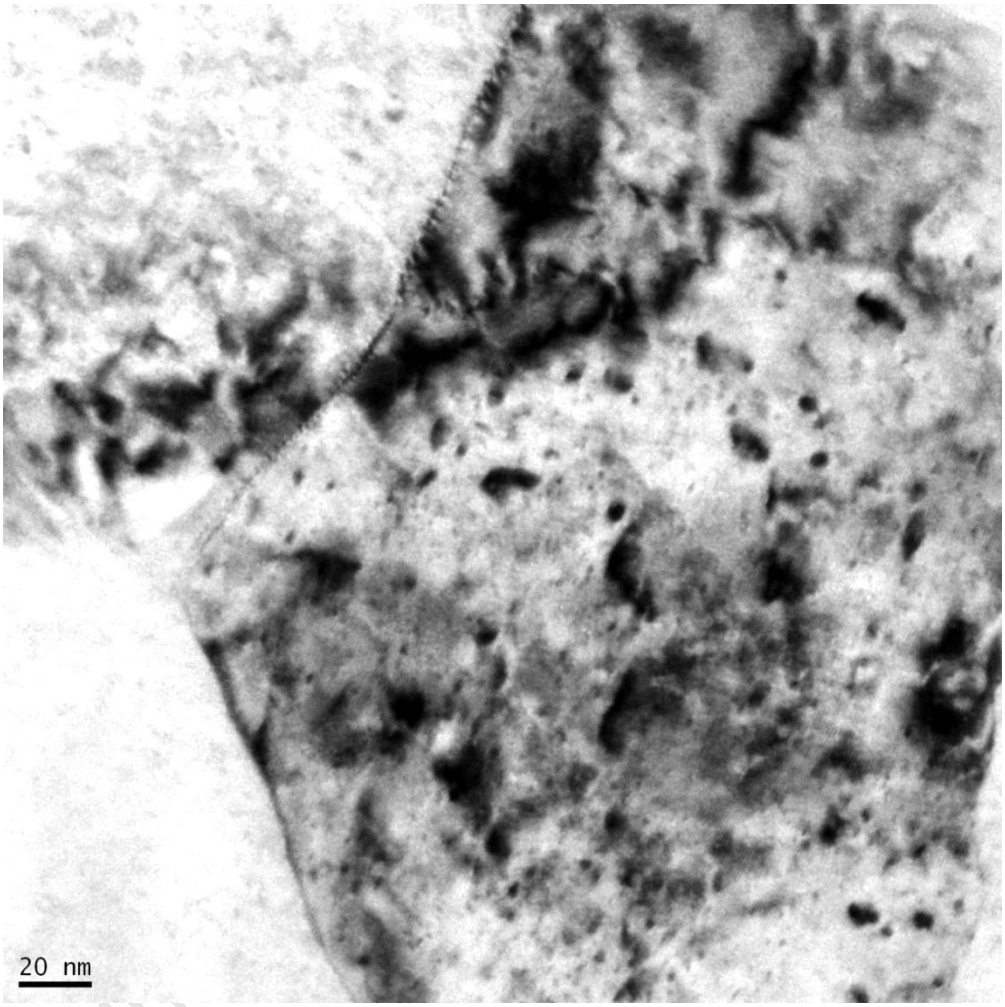

Figure 4.22: TEM image of heat treated 300 °C Pd 11.1 at.% Cu, showing grain boundaries.

Figure 4.22 and Figure 4.24 show TEM images of the Pd 11.1 at.% Cu alloy heat treated at 300 °C for 3 hours, with grain boundaries featured. Figure 4.23 and Figure 4.25 show ESI colour maps of Figure 4.22 and Figure 4.24 respectively, with Figure 4.23 and Figure 4.25 showing a concentration of copper on the grain boundaries. The ‘dark’ areas are regions of increased diffraction, and are caused by differing crystal orientations, dislocation strains or thickness fringes. Figure 4.26 shows a thickness map of Figure 4.24 where white indicates areas of higher thickness.

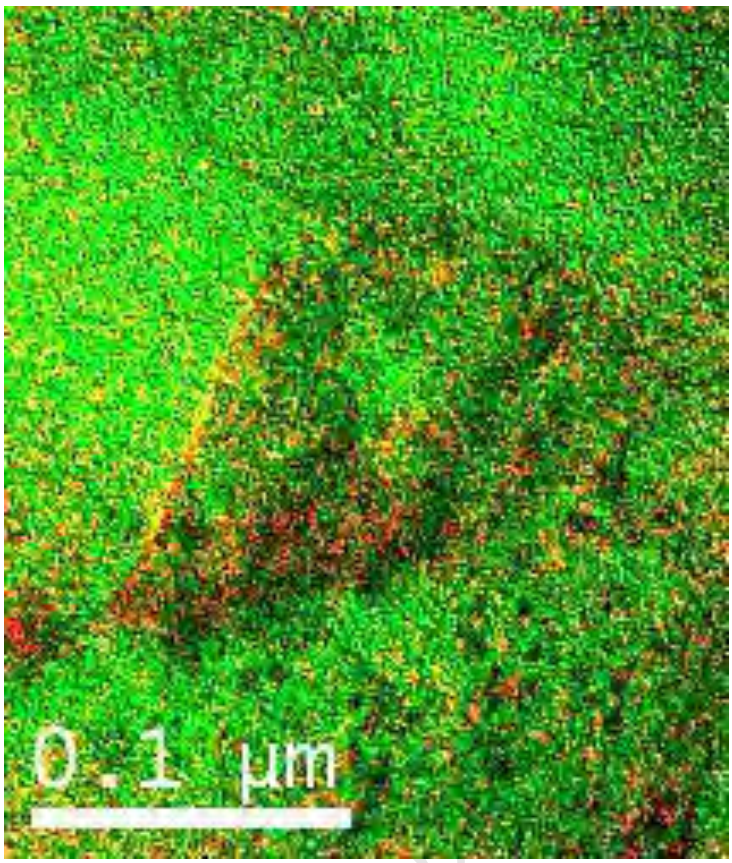

Figure 4.23: ESI colour map of Pd 11.1 at.% Cu heat treated at 300 °C for 3 hours (Green = Pd, Red = Cu).

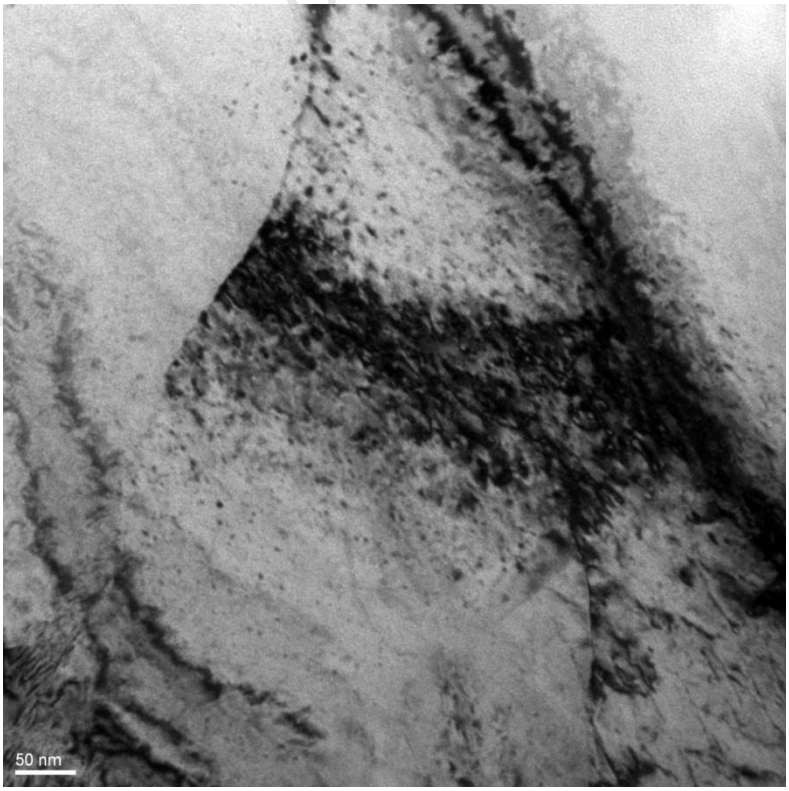

Figure 4.24: TEM image of Pd 11.1 at.% Cu heat treated at 300 °C for 3 hours, showing a grain boundary .

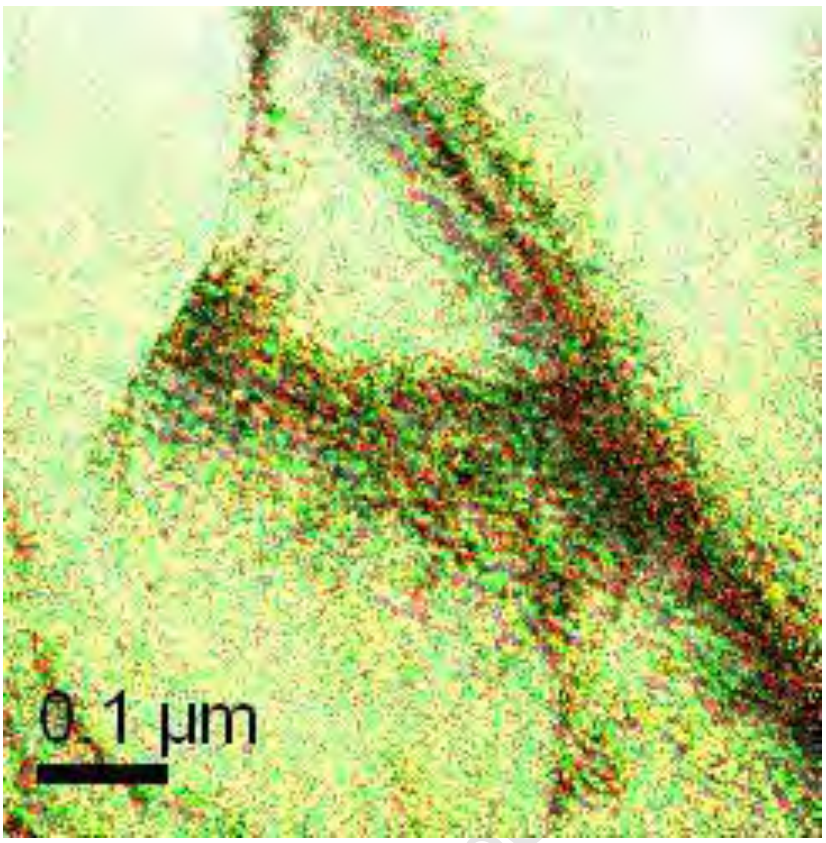

Figure 4.25: ESI colour map of Pd 11.1 at.% Cu heat treated at 300 °C for 3 hours (green = Pd, red = Cu).

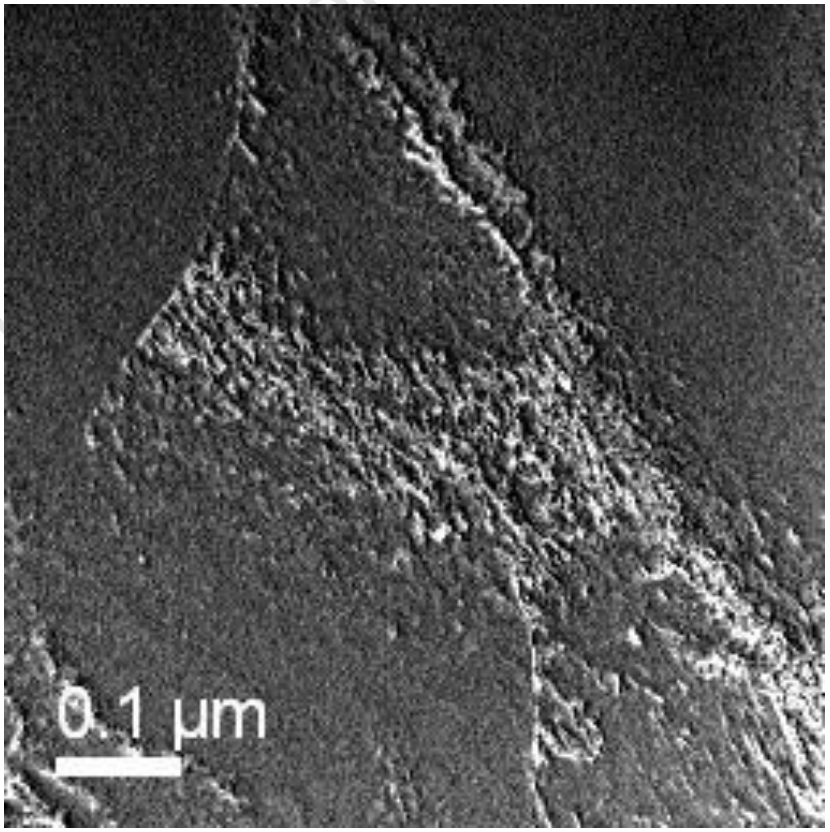

Figure 4.26: ESI thickness map of Pd 11.1 at.% Cu heat treated at 300 °C for 3 hours (increased thickness = white areas).

Figure 4.27 is a TEM image of the Pd 11.1 at.% Cu alloy heat treated at 700 °C for 3 hours, with a grain boundary shown. Figure 4.28 shows an ESI colour map of Figure 4.27, which shows no copper concentration near the grain boundary. For the area of increased diffraction above the grain boundary, we see some segregation of copper similar to what was seen in Figure 4.23 and Figure 4.25.

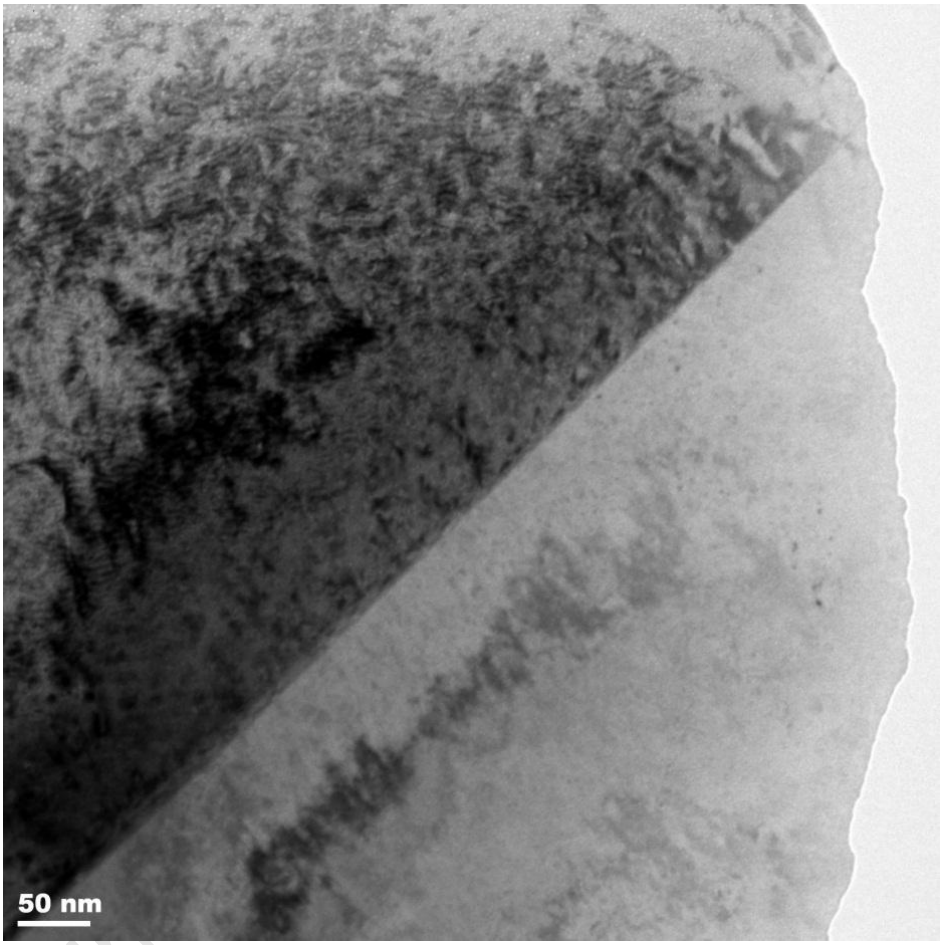

Figure 4.27: TEM image of Pd 11.1 at.% Cu heat treated at 700 °C for 3 hours, showing a grain boundary.

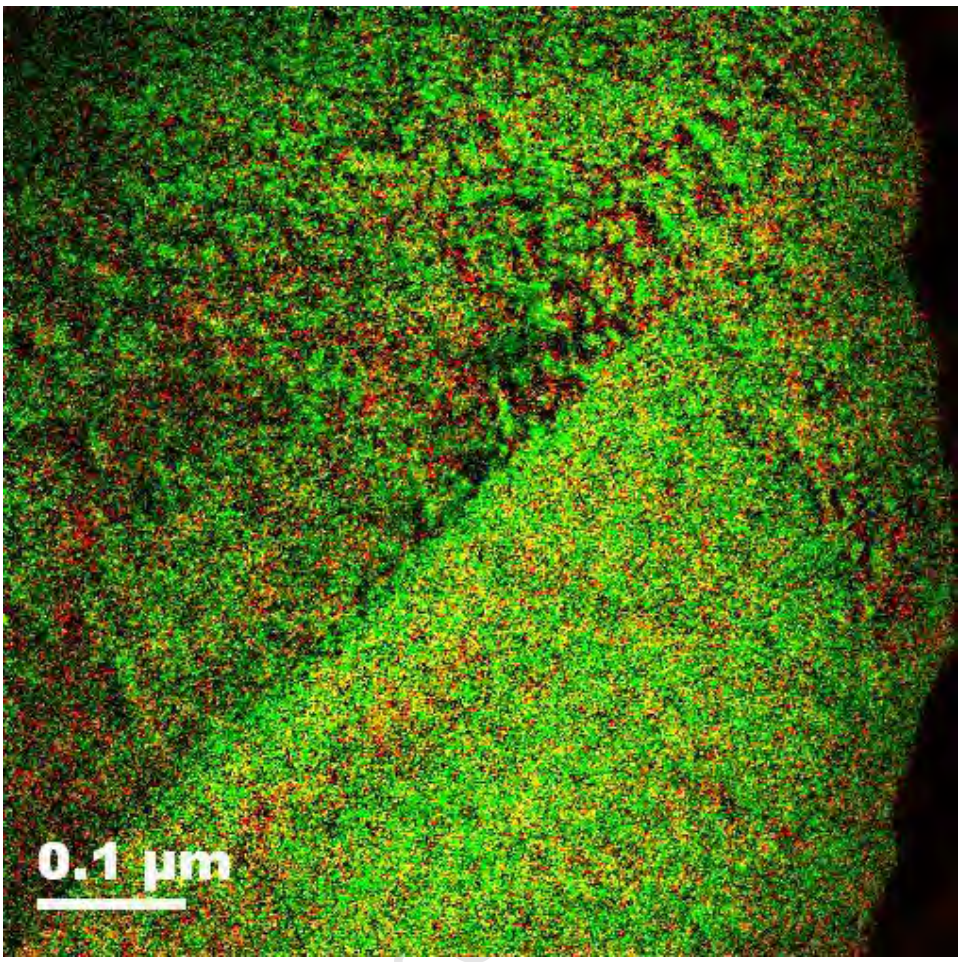

Figure 4.28: ESI colour map of Pd 11.1 at.% Cu heat treated at 700 °C for 3 hours (Green = Pd, Red = Cu).

4.2. Palladium-niobium

This section contains results for the palladium 11.1 atomic per cent niobium alloy.

4.2.1. Microhardness Measurements

Figure 4.29 shows the hardness of the Pd-Nb alloy after homogenisation (1200 °C for 1 week), the average hardness of the alloy was recorded as 197.4 HV. After a further 90% deformation the average hardness changed to 412.9 HV. The subsequent heat treatments did not have a significant effect on hardness when compared with the deformed (pre-heat treatment) sample.

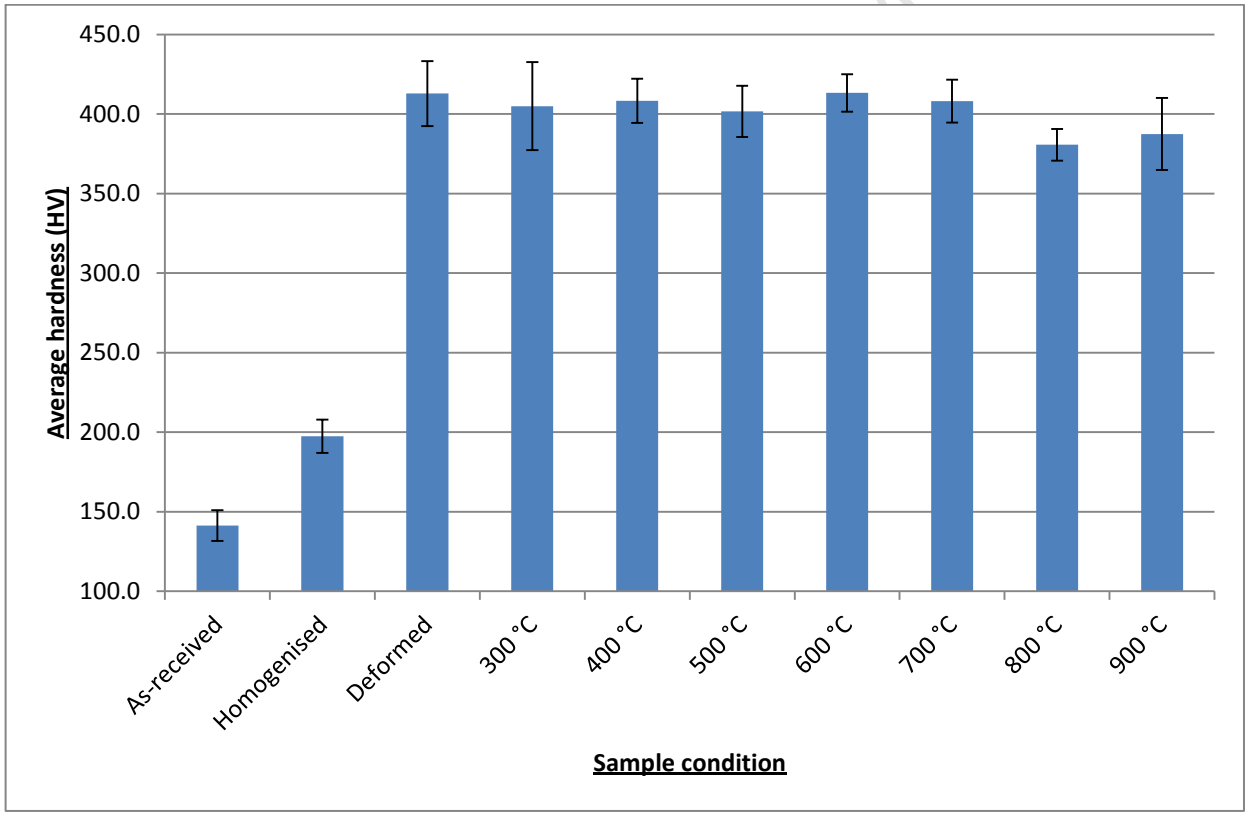

Figure 4.29: Average hardness for cold worked Pd-Nb alloy after heat treatments of 3 hours each.

Isothermal heat treatments were done at 600 °C for 1 week and 2 weeks, with the hardness results shown in Figure 4.30 with the deformed and heat treated at 600 °C for 3 hours average hardness results added for comparison. The hardness in Figure 4.30 shows no significant average hardness changes for the heat treated 600 °C for 3 hours, 1 week and 2 weeks samples when compared to the deformed sample.

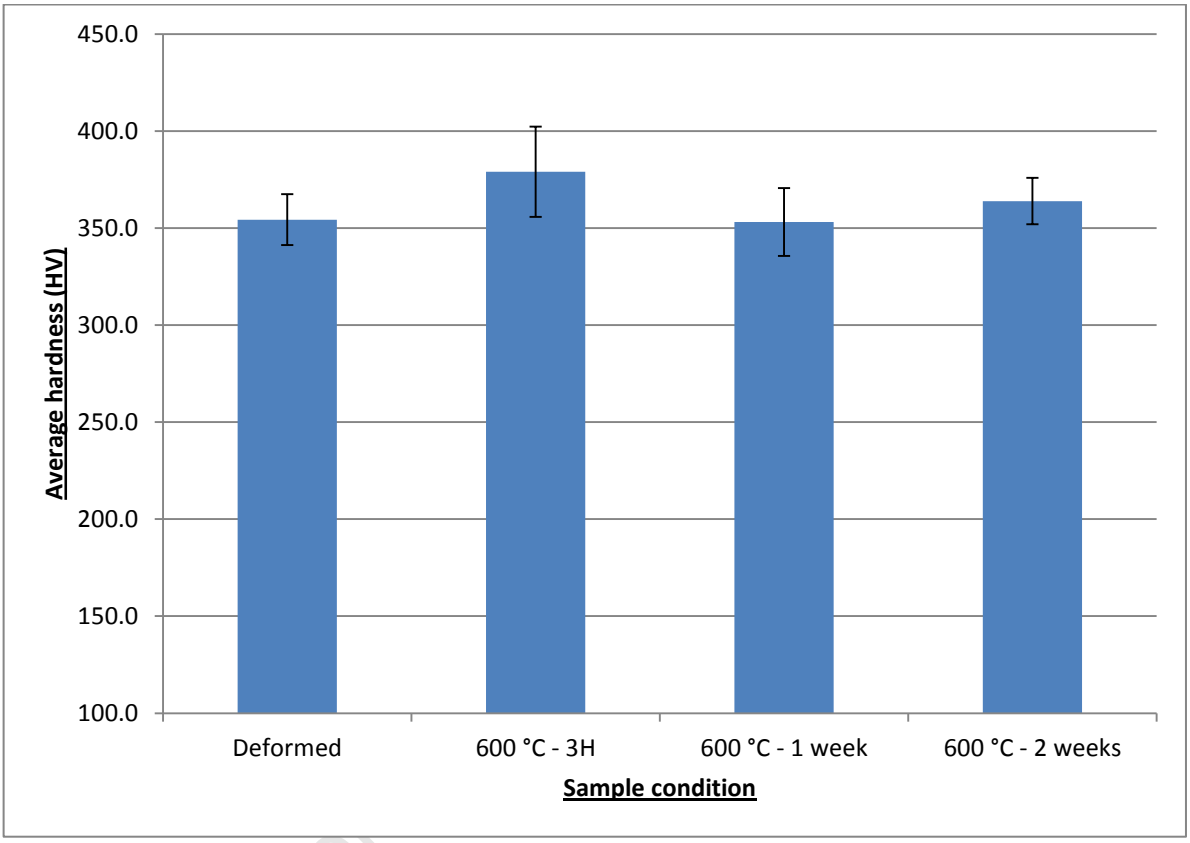

Figure 4.30: Average hardness for deformed Pd-Nb alloy after isothermal heat treatments at 600 °C each.

4.2.2. Light microscopy

Light micrographs were collected on the Pd 11.1 at.% Nb alloy for the deformed condition, heat treated at 300 °C for 3 hours, 600 °C for 3 hours, 900 °C for 3 hours, 600 °C for 1 week and 600 °C for 2 weeks (Figure 4.31, Figure 4.32, Figure 4.33, Figure 4.34, Figure 4.35 and Figure 4.36 respectively). All micrographs had evidence of a deformed structure remaining in their respective heat treatment, and a 'white' artefact was seen on some of the samples.

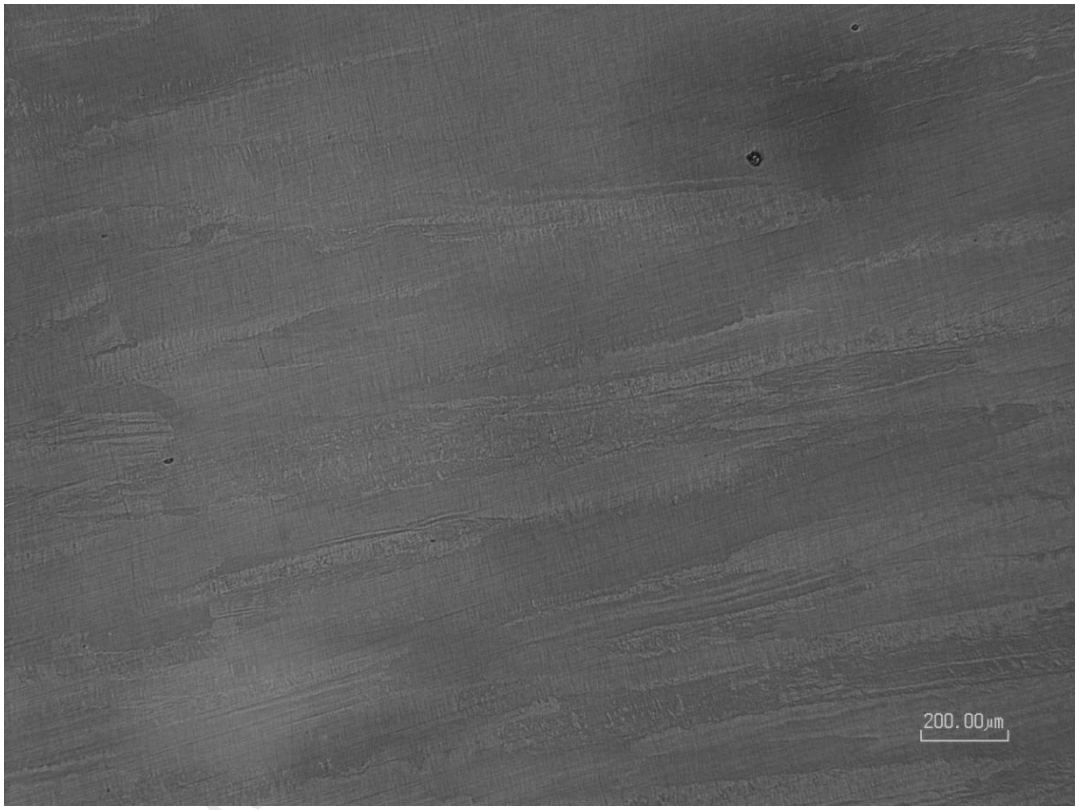

Figure 4.31: Micrograph of deformed Pd-Nb alloy before heat treatments.

Figure 4.32: Micrograph of Pd-Nb alloy after heat treatment at 300 °C for 3 hours.

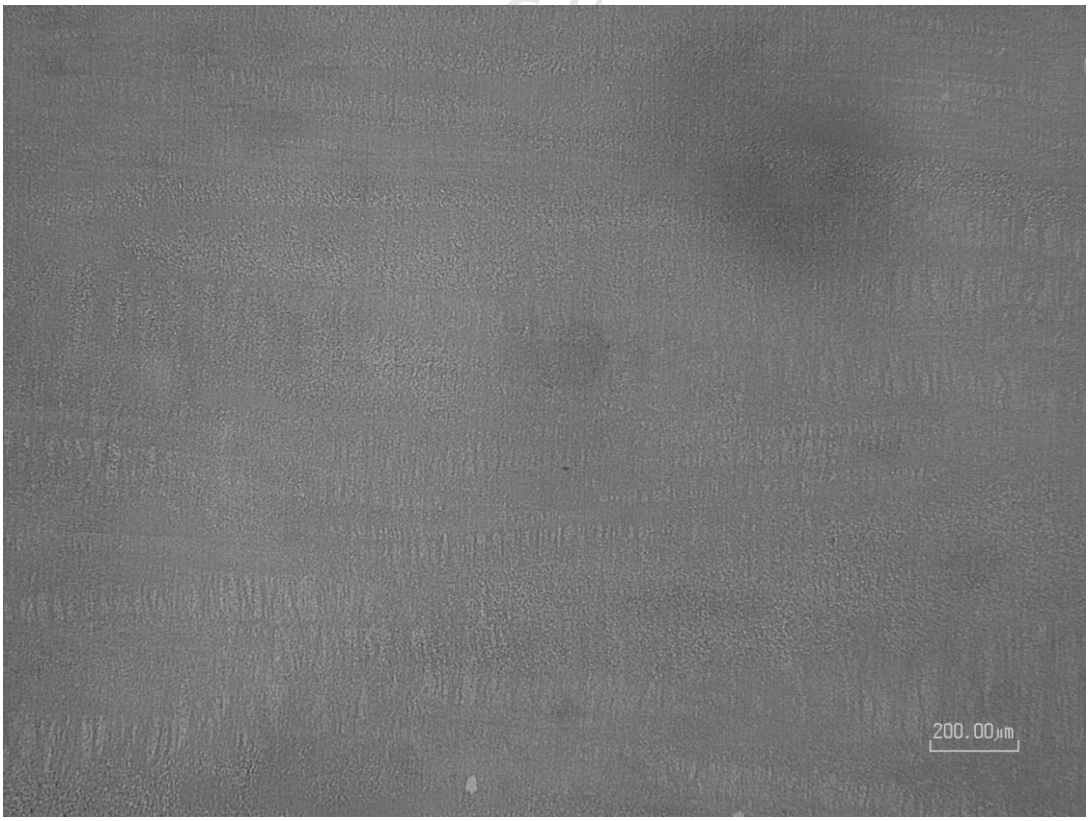

Figure 4.33: Micrograph of Pd-Nb alloy after heat treatment at 600 °C for 3 hours.

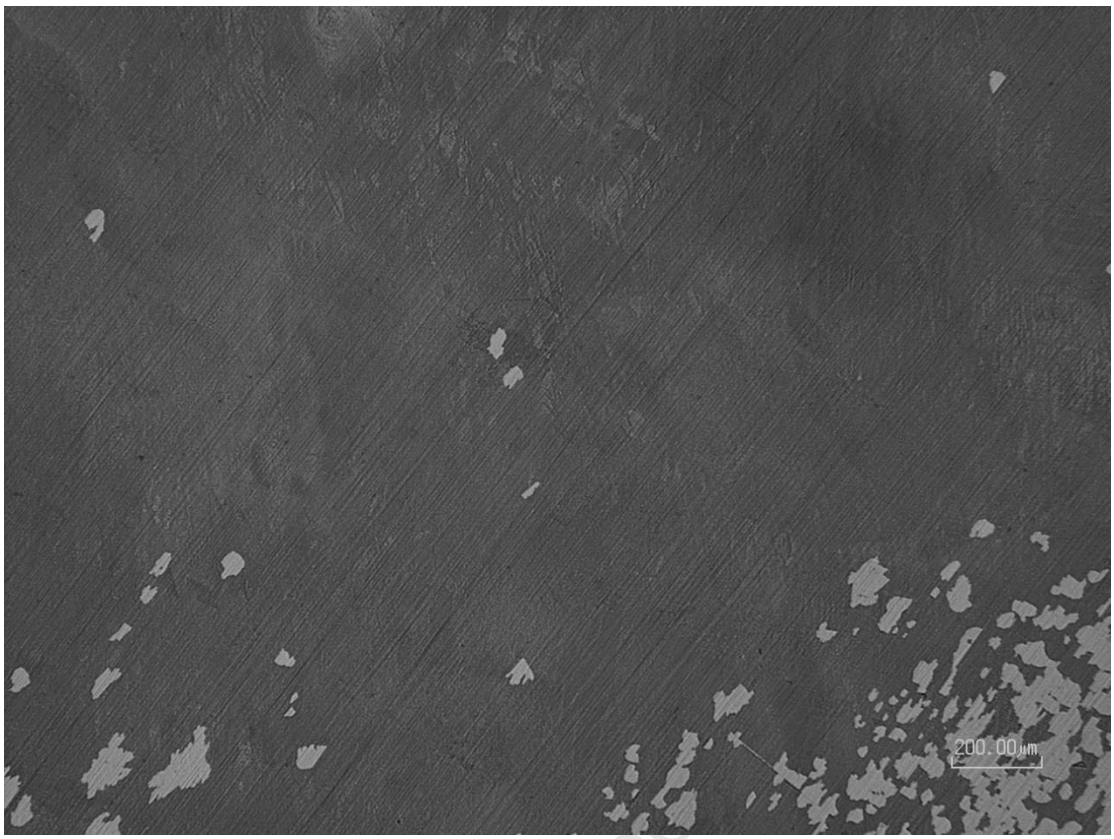

Figure 4.34: Micrograph of Pd-Nb alloy after heat treatment at 900 °C for 3 hours.

Figure 4.35: Micrograph of Pd-Nb alloy after heat treatment at 600 °C for 1 week.

Figure 4.36: Micrograph of Pd-Nb alloy after heat treatment at 600 °C for 2 weeks.

4.2.3. Differential Scanning Calorimetry

DSC was performed on the Pd 11.1 at.% Nb to determine if any thermodynamic changes could be detected for various temperatures. Figure 4.37 shows the DSC curve of a heat treatment of heating at 5 °K / min to 700 °C from room temperature (labelled [1.1] on Figure 4.37), then held at 700 °C for 3 hours, ending with a cooling to room temperature at 5 °K / min (labelled [1.3] on Figure 4.37). No peaks were seen on the heating cycle, and a very broad endothermic peak was seen at 675 °C during the cooling cycle.

A similar heating cycle is shown in Figure 4.38, for a sample heat treated to 800 °C at 5 °K / min with the heating cycle labelled [1.1] and the cooling cycle labelled [1.3]. The curves on Figure 4.37 and Figure 4.38 appear to be almost identical, with similar shape and values.

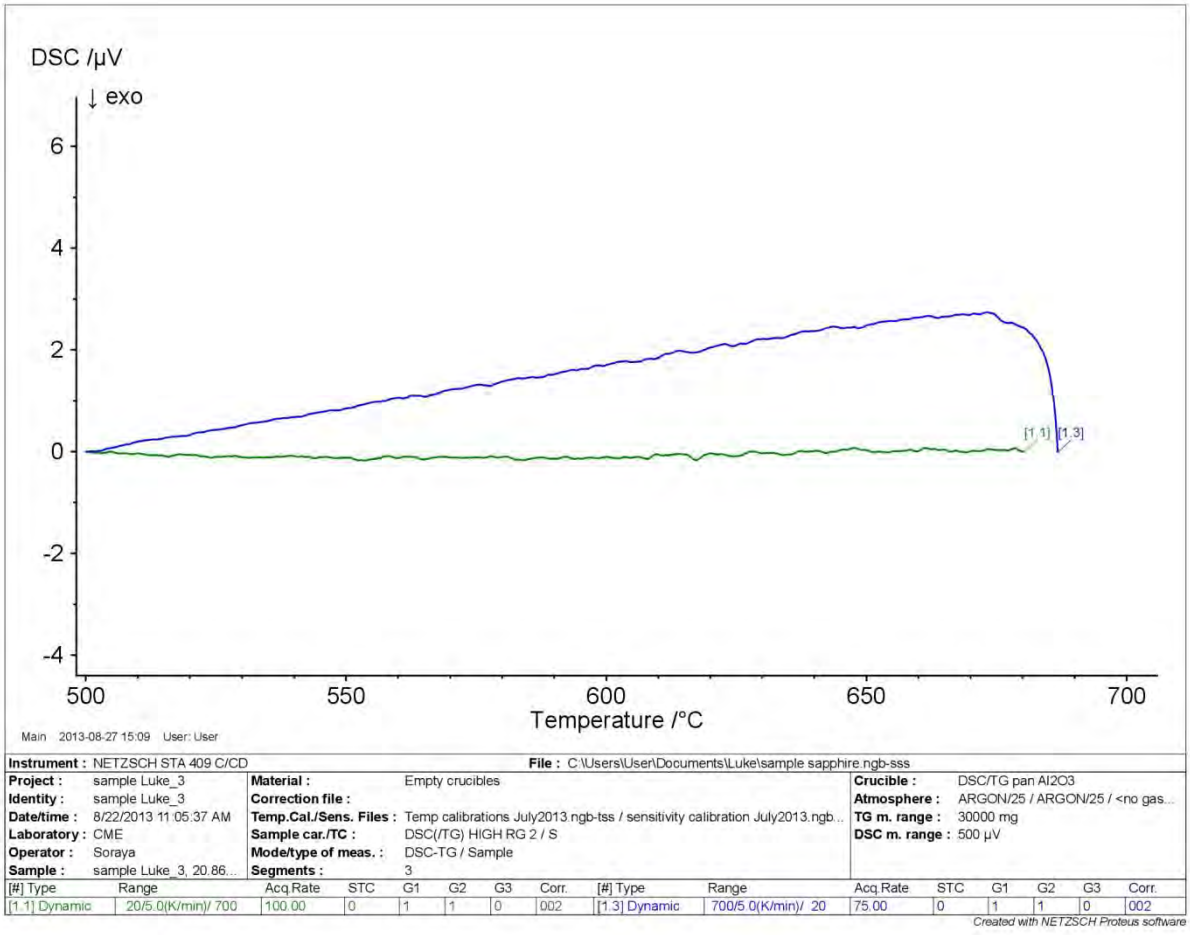

Figure 4.37: DSC curve of Pd-Nb alloy heat treated to 700 °C for 3 hours.

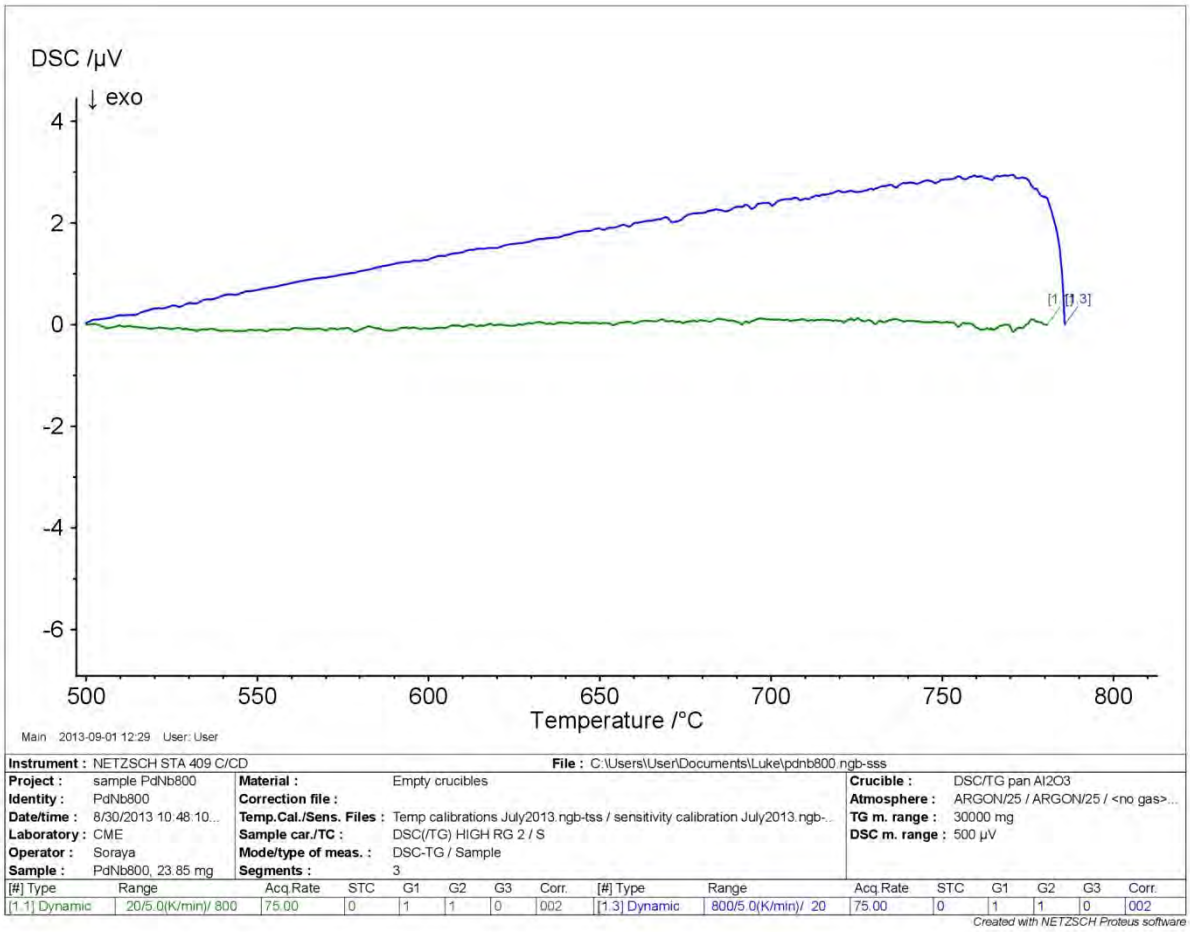

Figure 4.38: DSC curve of Pd-Nb alloy heat treated to 800 °C for 3 hours.

4.2.4. SEM/EDS

The Pd 11.1 at.% Nb alloy was analysed under SEM-EDS in a similar manner as the Pd 11.1 at.% Cu alloy (see section 4.1.3) and showed no unusual surface features, and showed the composition was as expected for the Pd 11.1 at.% Nb alloy.

5. Discussion

5.1. Pd 11.1 at.% Cu

The hardness results of the isochronal heat treatments of 3 hours each on initially deformed samples (as shown on Figure 4.1) showed no significant hardness changes for heat treatments 100 °C, 200 °C and 300 °C when compared with the deformed sample, while a decreasing trend in hardness begins from heat treatments 400 °C to 700 °C where after for heat treatments 800 °C and 900 °C the hardness is very similar to the 700 °C heat treatment. This hardness profile does not show similar hardening behaviour which has been seen after heat treatment of other alloys[7,15,16,23], where an increase in hardness was detected at moderate heat treatment temperatures, and the increase in hardness was attributed to ordering.

Instead the hardness profile gathered here for the Pd 11.1 At.% Cu alloy suggests a typical recovery and recrystallization hardness pattern, which is also supported by the micrographs as a recrystallized (refined equiaxed) grain structure is seen in the heat treated 700 °C for 3 hours sample (Figure 4.8) and the heat treated 900 °C for 3 hours sample (Figure 4.9). The point at which recovery takes place is harder to detect as initially very little change occurs for the grain structure making metallographic detection difficult. Recovery was conjectured to begin around or shortly after the heat treated 400 °C for 3 hours sample as a decreasing trend in hardness was noted.

Similarly for the hardness profile of the isochronal initially quenched samples (Figure 4.2) and isothermal heat treatments at 300 °C (Figure 4.3), both show a hardness trend comparable to the hardness profile of Figure 4.1 where no significant hardness changes occur at low heat treatment temperatures or heat treatment times respectively, followed by a decreasing trend in hardness relative to increasing heat treatment temperature or increasing heat treatment time respectively.

SEM-EDS indicated that the alloy used in this work was near the expected composition and detected no significant compositional changes for the samples heat treated at 200 °C for 3 hours, 300 °C for 3 hours, 400 °C for 3 hours and 700 °C for 3 hours.

TEM-ESI on the sample heat treated at 300 °C for 3 hours (Figure 4.22, Figure 4.23, Figure 4.24 and Figure 4.25), indicates that copper had migrated to the grain boundary, but Figure 4.24 and Figure 4.25, also indicates that copper had migrated to areas of higher diffraction (darker areas). These areas of higher diffraction were seen as an area of increased thickness when a thickness map was applied (highlighted white in Figure 4.26).

This phenomenon of solute atom migration is well known as equilibrium segregation, as the solute atoms migrate to areas of higher energy (such as grain boundaries and defects) in order to decrease the Gibbs free energy of the system[57,58]. The scale of the solute atom migration may also not be significant enough to cause noticeable hardness changes for the sample and fits with the microhardness data shown in Figure 4.1. For the sample heat treated at 700 °C for 3 hours (Figure 4.27) the grain boundary did not have the migration of copper (Figure 4.28) but the area of increased diffraction still showed some migration of copper.

This lack of solute atom migration to the grain boundary fits with the hardness profile of Figure 4.1 and the metallographic image (Figure 4.8) of the sample heat treated at 700 °C for 3 hours as they all indicate that recrystallization has occurred for this heat treatment.

TEM diffraction analysis was carried out on a sample heat treated at 300 °C for 3 hours (Figure 4.21). No extra reflections were noted on the zone axes investigated, and this matches the no extra reflections seen on the deformed sample (Figure 4.20). The present experimental work suggests no ordered structure was formed from heat treatments ranging from 100 °C to 900 °C for 3 hours each, including the heat treatments at 300 °C for extended heat treatment length (up to 48 hours). The detection of no ordering transformation within the temperature range of 100 °C to 900 °C is consistent with the prediction by Carr *et al*[2] of a T_c of -150 °C for the ordered structure.

5.2. Pd 11.1 at.% Nb

The hardness profile of Pd 11.1 at.% Nb alloy yielded no significant hardness changes, for the initially deformed heat treated samples ranging from 300 °C to 900 °C of 3 hours each (Figure 4.29), when compared with the deformed sample. The samples heat treated at 600 °C with increased heat treatment times of 1 week and 2 weeks (Figure 4.30) showed no significant changes when compared against the hardness of the deformed sample. This does not match the hardness profiles seen from after heat treatment of other alloys[7,15,16,23], where an increase in hardness was attributed to ordering.

The micrographs of the isochronal heat treated samples showed evidence of a deformed microstructure up to the heat treatment at 900 °C for 3 hours. This assists in explaining why the hardness results show very little change for their respective heat treatments, as no significant microstructural changes have possibly occurred. There was some difficulty with the etchant used, as it caused an undesired artefact to form on the surface which partially obscured the revealing of the microstructure. This lead to some uncertainty with the microstructural results but still did appear to partially explain the hardness results, as the microstructure that could be seen appeared to still be in the deformed state for all heat treated samples.

The SEM-EDS analysis showed no unusual surface features or composition variance from what was expected. DSC analysis was used for samples heat treatments at 700 °C for 3 hours and 800 °C for 3 hours (Figure 4.37 and Figure 4.38 respectively). The DSC curves seen on Figure 4.37 and Figure 4.38 are similar in shape and values, with no narrow peaks along the curves. This suggests that no phase transformation has occurred for those heat treatments.

Carr *et al*[2] predicted an A_8B superlattice with a T_c of 725 °C at the Pd 11.1 at.% Nb composition, we would expect the ordering to occur at 725 °C or below. No significant hardness changes were seen from the selected heat treatments, especially near the samples heat treated at 600 °C for 3 hours and 700 °C for 3 hours which would indicate possible ordering had occurred. This was further backed up by the lack of unusual surface features noted in the light microscopy and SEM images. DSC analysis also further suggests no ordering has occurred as no narrow peaks were noted on the curves, which would indicate a phase transformation had occurred.

The issue facing the Pd 11.1 at.% Nb alloy may be due to its thermodynamics as Giessen *et al*[51] has indicated that homogenisation treatments of 800 °C require a heat treatment length of at least 2 months thus for the possible ordering of Pd_8Nb to occur an estimated heat treatment length of 8 months or more may be required, taking into account that a sufficiently undercooled sample below 725 °C would be required. This poses some experimental difficulty as oxidation could be a limiting factor.

6. Conclusions

The method of using prior deformation with subsequent heat treatments to produce ordering, as used in other work[7,15,16,23], was not sufficient to produce ordering in both alloys for their respective heat treatments. For the Pd 11.1 at.% Cu alloy, while no significant hardness changes where seen in Figure 4.1 the heat treated at 300 °C for 3 hours sample gave the highest hardness result relatively, and was further characterized by TEM examination. The TEM examination suggested no ordering for the selected heat treated at 300 °C for 3 hours sample. For the Pd 11.1 at.% Nb alloy we expected possible ordering to occur below the theorised T_c of 725 °C[2], but the selected heat treatments were not thermodynamically favourable to promote ordering, even with prior deformation added to create extra energy for atomic rearrangement.

7. Recommendations

To produce the ordering in the Pd 11.1 at.% Cu alloy, an experimental difficulty must be overcome. Rapid cooling to temperatures lower than -150 °C while possible presents a problem, as these low temperatures are not sufficient for atomic rearrangement to occur. Possibly by coupling rapid cooling with a sample that has undergone proton irradiation to create excess vacancies might be sufficient.

Similarly for the Pd 11.1 at.% Nb alloy, proton irradiation may be used to generate excess vacancies which may overcome the energy barrier preventing sufficient atomic rearrangement. This may lead to the theorised Pd_8Nb ordering.

A solution for the problem on etching the Pd 11.1 at.% Nb alloy may also be investigated, to provide better analysis of the microstructure.

The oxidation problems of long heat treatments of the Pd 11.1 at.% Nb alloy may be eliminated by using a vacuum furnace that is capable of replacing the atmosphere with an inert gas, such as Argon.

8. References

1 G. L. W. Hart, *Nature Mater.,* 2007, **6**, 941-945.

2 D. A. Carr, J. Corbitt, G. R. Hart, E. Gilmartin and G. L. W. Hart, *Comp. Mat. Sci.,* 2011, **51**, 331-339.

3 Z. W. Lu and B. M. Klein, *Phys.Rev.B,* 1994, **50**, 5962-5970.

4 C. S. Barrett and T. B. Massalski, *Structure of metals: crystallographic methods, principles and data*, Pergamon, Oxford New York, 1980.

5 R. S. Irani, *Contemp. Phys.,* 1972, **13**, 559-583.

6 R. S. Irani and R. W. Cahn, *Acta Metall.,* 1973, **21**, 575-584.

7 N. S. Stoloff and R. G. Davies, *Prog Mater Sci,* 1966, **13**, 1-84.

8 J. Cheng and A. J. Ardell, *Acta Metall.,* 1989, **37**, 1891-1902.

9 ASM International, *Binary alloy phase diagrams second edition*, Materials Park, OH : ASM International, 1996.

10 D. G. Pettifor, *J. Phys. C: Solid State Phys.,* 1986, **19**, 285-313.

11 S. Curtarolo, D. Morgan and G. Ceder, *Computer Coupling of Phase Diagrams and Thermochemistry,* 2005, **29**, 163-211.

12 S. Curtarolo, D. Morgan, K. Persson, J. Rodgers and G. Ceder, *Phys. Rev. Lett.,* 2003, **91**, 135503-1-135503-4.

13 C. C. Fischer, K. J. Tibbits, D. Morgan and G. Ceder, *Nature Mater.,* 2006, **5**, 641-646.

14 G. L. W. Hart and R. W. Forcade, *Phys. Rev. B,* 2008, **77, 224115**, 1-12.

15 S. Nxumalo, M. P. Nzula and C. I. Lang, *Mat. Sci. Eng. A,* 2007, **445-446**, 336-340.

16 M. P. Nzula, C. I. Lang and D. J. H. Cockayne, *J. Alloys Compd.,* 2006, **420**, 165-170.

17 H. Lang, T. Mohri and W. Pfeiler, *Intermetallics,* 1999, **7**, 1373-1381.

18 W. Pfeiler and B. Sprusil, *Mat. Sci. Eng. A,* 2002, **324**, 34-42.

19 B. Schönfeld, *Prog. Mater. Sci.,* 1999, **44**, 435-543.

20 T. Pretorius and E. Nembach, *Acta Mater,* 1999, **47**, 1953-1964.

21 L. Trieb and G. Veith, *Acta Metall.,* 1978, **26**, 185-196.

22 J. S. Koehler, *Phys. Rev. B,* 1970, **2**, 547-551.

23 M. Carelse and C. I. Lang, *Scripta Mater.,* 2006, **54**, 1311-1315.

24 E. Nembach, *Prog. Mater. Sci.,* 2000, **45**, 275-338.

25 A. Kulovits, J. M. K. Wiezorek, W. A. Soffa, W. Püschl and W. Pfeiler, *J. Alloys Compd.,* 2004, **378**, 285-289.

26 F. C. Larche, *Dislocations in Solids: Dislocations in metallurgy*, edited by F. R. N. Nabarro, North Holland, Amsterdam, 1979, 135-154.

27 M. Migschitz, A. Korner, W. Garlipp and W. Pfeiler, *Acta Mater.,* 1996, **44**, 2821-2829.

28 W. Pfeiler, R. Kozubskip, H. P. Karnthaler and C. Rentenberger, *Acta Mater.,* 1996, **44**, 1563-1571.

29 S. Harper, *Phys. Rev.,* 1951, **83**, 709-712.

30 NRL crystal structure website. http://cst-www.nrl.navy.mil/lattice/, 19/10/2010.

31 Y. Tang, *Acta Cryst.,* 1951, **4**, 377-378.

32 P. Pietrokowsky, *Nature,* 1965, **206**, 291.

33 D. Schryvers and S. Amelinckx, *Res. Mech.,* 1987, **22**, 101-149.

34 W. E. Quist, van der Wekken, C. J., R. Taggart and D. H. Polonis, *Trans. TMS-AIME,* 1969, **245**, 345-349.

35 S. Nxumalo and C. I. Lang, *J. Alloys Compd.,* 2006, **425**, 181-184.

36 E. Savitsky, V. Polyakova, N. Gorina and N. Roshan, *Physical Metallurgy of Platinum Metals*, Mir Publishers, Moscow, 1978.

37 C. J. Smithells and E. A. Brandes, *Metals reference book*, Butterworths, London, 1967.

38 L. B. Hunt and F. M. Lever, *Platinum Met. Rev.,* 1969, **13**, 126-138.

39 J. Matthey, *Platinum 2009 Interim Review*, Platinum 2009, 2009.

40 M. Winter. http://www.webelements.com/niobium/, 11/24/2011.

41 M. Winter. http://www.webelements.com/copper/, 11/24/2011.

42 W. Grochala and P. P. Edwards, *Chem. Rev.,* 2004, **104**, 1283-1315.

43 K. Ohshima and D. Watanabe, *Acta Cryst.,* 1973, **A29**, 520-526.

44 A. Schneider and U. Esch, *Z. Elektrochem. Angew. Phys. Chem.,* 1944, **50**, 290-301.

45 P. R. Subramanian and D. E. Laughlin, *J. Phase Equil.,* 1991, **12**, 231-243.

46 M. Hansen and K. Anderko, *Constitution of Binary Alloys*, McGraw-Hill, New York, 1958.

47 D. K. Saha, K. Koga and K. Ohshima, *J. Phys. : Condens. Matter,* 1992, **4**, 10093-10102.

48 S. Baerthlein, E. Winning, G. Hart and S. Mueller, *Acta Mater.,* 2009, **57**, 1660-1665.

49 Y. Sato, J. M. Sivertsen and L. E. Toth, *Phys.Rev.B,* 1970, **1**, 1402-1410.

50 K. M. Myles and J. B. Darby Jr., *Acta Metall.,* 1968, **16**, 485-492.

51 B. C. Giessen, N. J. Grant, D. P. Parker, R. C. Manuszewski and R. M. Waterstrat, *Met. Trans. A,* 1980, **11A**, 709-715.

52 J. C. Anderson, *Materials Science*, Van Nostrand Reinhold, Berkshire, England, 1985.

53 S. Nxumalo and C. I. Lang, *J. Phys. : Conf. Ser.,* 2008, **126**, 1-4.

54 J. Naser, W. Riehemann and H. Ferkel, *Mater. Sci. Eng. A,* 1997, **234-236**, 467-469.

55 H. T. Stokes and B. J. Campbell, *ISOCIF,* 2006, **Department of Physics and Astronomy**, Brigham Young University, Provo, Utah.

56 J. M. Zuo and J. C. Mabon, *Microsc. Microanal.,* 2004, **10 (Suppl. 2)**, URL: http://emaps.mrl.uiuc.edu/.

57 S. Hofmann and P. Leiĉek, *Interface Sci.,* 1996, **3**, 241-267.

58 R. N. Barnett, U. Landman and C. L. Cleveland, *Phys. Rev. B,* 1983, **28**, 6647-6658.